Malformations of Cortical Development: Updated Imaging Review

Julia M. Brunelli, MD • Thiago J. P. Lopes, MD* • Isabela S. Alves, MD • Daniel S. Delgado, MD • Hae W. Lee, MD, PhD • Maria G. M. Martin, MD, PhD*
Marcos F. L. Docema, MD • Samya S. Alves, MD • Paula C. Pinho, MD • Vinicius T. Gonçalves, MD • Lucas R. L. B. Oliveira, MD
Jorge T. Takahashi, MD • Pejman J. Maralani, MD • Camila T. Amancio, MD • Claudia C. Leite, MD, PhD

*J.M.B and T.J.P.L contributed equally to this work.
Author affiliations, funding, and conflicts of interest are listed at the end of this article.

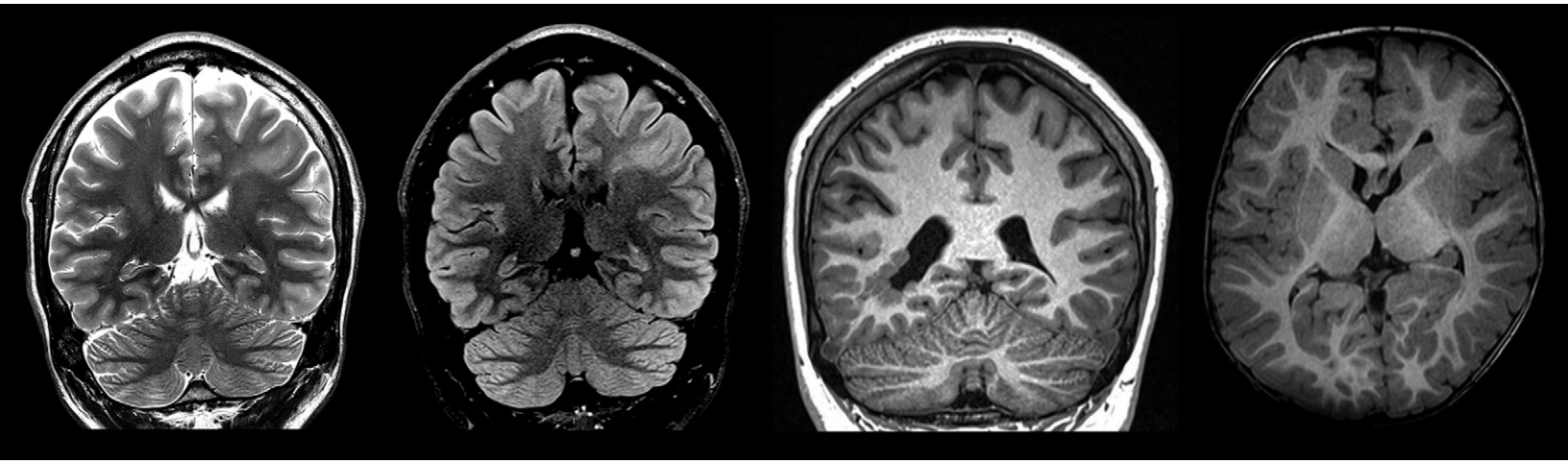

Malformations of cortical development (MCD) are structural anomalies that disrupt the normal process of cortical development. Patients with these anomalies frequently present with seizures, developmental delay, neurologic deficits, and cognitive impairment, resulting in a wide spectrum of neurologic outcomes. The severity and type of malformation, in addition to the genetic pathways of brain development involved, contribute to the observed variability. While neuroimaging plays a central role in identifying congenital anomalies in vivo, the precise definition and classification of cortical developmental defects have undergone significant transformations in recent years due to advances in molecular and genetic knowledge. The authors provide a concise overview of embryologic brain development, recently standardized nomenclature, and the categorization system for abnormalities in cortical development, offering valuable insights into the interpretation of their neuroradiologic patterns.

Introduction

Malformations of cortical development (MCD) are structural abnormalities that interfere with the normal corticogenesis process. The definite incidence of MCD is unknown. Patients with MCD may exhibit a wide range of clinical symptoms, from asymptomatic cases to severe manifestations such as intractable epilepsy, developmental delay, neurologic deficits, and cognitive impairment.

A varied etiology can be associated with MCD. Errors, caused by gene mutations, infections, or environmental insults, can occur at any time in the cortical development process, resulting in diverse manifestations. In recent years, unprecedented progress has been made in the identification of genes and signaling pathways that frequently cause cortical malformations. Given that the definitive diagnosis of MCD is typically based on histopathologic findings and that obtaining pathologic tissue is often problematic, neuroimaging plays a crucial role in assessment of these patients.

Fetal US or MRI can help identify some MCD in utero, such as lissencephaly (LIS), polymicrogyria (PMG), cobblestone malformation (Fig 1), or large heterotopia. However, MCD are typically a postnatal diagnosis, and MRI is the preferred method to investigate this condition (1). In addition to neuroimaging, clinical phenotyping and genetic studies are essential diagnostic tools.

Review of Cortical Development

Neurogenesis

The cerebral cortex is formed by neuroepithelial cells (NECs). In the 4th week of development, neural plate NEC proliferation occurs. Until neural tube closure has occurred, NECs

Supplemental Material

TestYour Knowledge

CME Slide Presentation

RadioGraphics 2024; 44(11):e230239
https://doi.org/10.1148/rg.230239

Content Codes: MR, NR

Abbreviations: FCD = focal cortical dysplasia, FLAIR = fluid-attenuated inversion recovery, LIS = lissencephaly, MCD = malformations of cortical development, PMG = polymicrogyria, SBH = subcortical band heterotopia

TEACHING POINTS

- A normal cortex at MRI should have these imaging features: *(a)* a normal external cortical surface and a smooth and sharply delineated cortico-subcortical junction and *(b)* sulci that may show slight anatomic variations but are uniform and symmetric in their position and depth.
- Imaging studies of patients with microcephaly primary hereditary traditionally show normal or simplified cortical gyral patterns, without severe malformations. A *simplified gyral pattern* is defined as a reduced number of gyri with shallow sulci (one-quarter to one-half of normal depth) but with normal thickness of the cerebral cortex at brain MRI.
- It is important to differentiate megalencephaly from macrocephaly. *Macrocephaly* (or macrocrania) is defined as an occipitofrontal circumference equal to or more than 2 SDs above the mean, whereas megalencephaly refers to a primarily developmental brain disorder associated with an abnormally large brain size.
- It is important to distinguish between periventricular nodular heterotopia and tuberous sclerosis subependymal nodules. The latter are positioned perpendicular to the ventricular walls, are not isointense to gray matter, frequently calcify, and may have enhancement after contrast agent administration.
- The resulting cortical phenotype will depend on the size of the gaps in the pial limiting membrane and the quantity of neurons that migrate to the subarachnoid space. Small gaps that lead to small clumps of neurons on the cortical surface are called polymicrogyria (PMG), while large gaps that lead to relatively smooth layers of neurons on the cortical surface define cobblestone malformation.

proliferate symmetrically (one stem cell divides into two stem cells), as shown in Figure 2 (2). Beginning at 8 weeks gestation and continuing until the end of the second trimester, some stem cells undergo neurogenesis, a process in which a stem cell generates a glial cell or neuron. Neuronal cells are generated earlier than glial cells (that originate oligodendrocytes and astrocytes) (3). This process occurs in the ventricular zone in the subependymal area of the lateral ventricles.

Neuronal proliferation reaches its peak between 15 and 16 weeks gestation, and it is believed that at least twice as many neurons are produced than required, and excess cells undergo apoptosis (4).

Neuronal Migration

The second stage occurs mainly from 12 to 20 weeks gestation, and neuronal migration happens in two distinct patterns: radial or tangential.

Radial migration leads the excitatory pyramidal neurons to the cortex surface in the newborn, and it is supported by radial glial cells. Radial glial cells extend from the subventricular zone to the pial surface at the external cortical border, providing a scaffold for neurons. The neurons that will form the brain layer migrate first, followed by the ones that will form the sixth, fifth, fourth, third, and second layers, forming

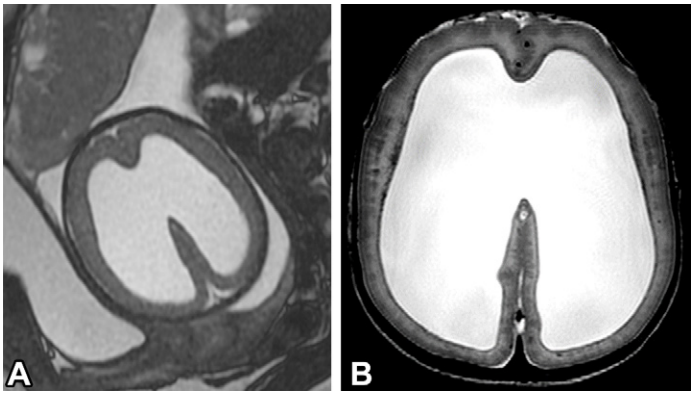

Figure 1. Cobblestone cortical malformation in a female infant. Axial T2-weighted fetal **(A)** and postnatal **(B)** MR images show a thickened and "pebbled" cerebral cortex, with a reduced sulcation and gyration pattern and ventriculomegaly.

the hexalaminar adult neocortex cytoarchitecture. The pial membrane prevents neuronal overmigration outside the external brain surface (5).

Tangential migration is responsible for cortical GABAergic interneurons in the cerebral cortex. These interneurons originate in the ganglionic eminences and migrate tangentially into the cortical plate, guided by axon projections and interstitial molecules (6).

Postmigration Neuronal Development

Postmigration neuronal development starts at 22 weeks gestation and lasts until 2 years of age. This stage is a complex process that results in the maturation of the six-layered cortex, outgrowth of axons and dendrites from the cortical neurons, and development of interneuronal synapses (7). The operculization, sulcation, and gyration processes are seen at this stage.

Review of Cortical Anatomy and Normal Imaging Findings

The cerebral cortex (gray matter) covers the outermost part of the brain and is composed of a complex arrangement of densely packed neuron cell bodies. The brain's enfolding is a reflex of the significant increase in brain size during evolution. Populations of neurons are interconnected via fibers that extend from each neuron's cell body and are represented by axons and dendrites. The histologic structure of the homotypical cerebral cortex consists of a laminar organization of six well-defined layers: *(a)* molecular (plexiform), *(b)* external granular, *(c)* external pyramidal, *(d)* internal granular, *(e)* internal pyramidal, and *(f)* multiform (polymorphous).

The phylogenetic classification of the cerebral cortex divides it into two parts: isocortex (also called neocortex) and allocortex, which is further divided into archicortex (ie, hippocampus, entorhinal cortices, and a cortical band of the cingulate gyrus) and paleocortex (ie, prepiriform and piriform regions, part of the amygdala, olfactory cortex, olfactory bulb, and septal regions). The isocortex covers almost the entire surface of the cerebral cortex and appeared later in the phylogenetic scale, consisting of all six histologic layers;

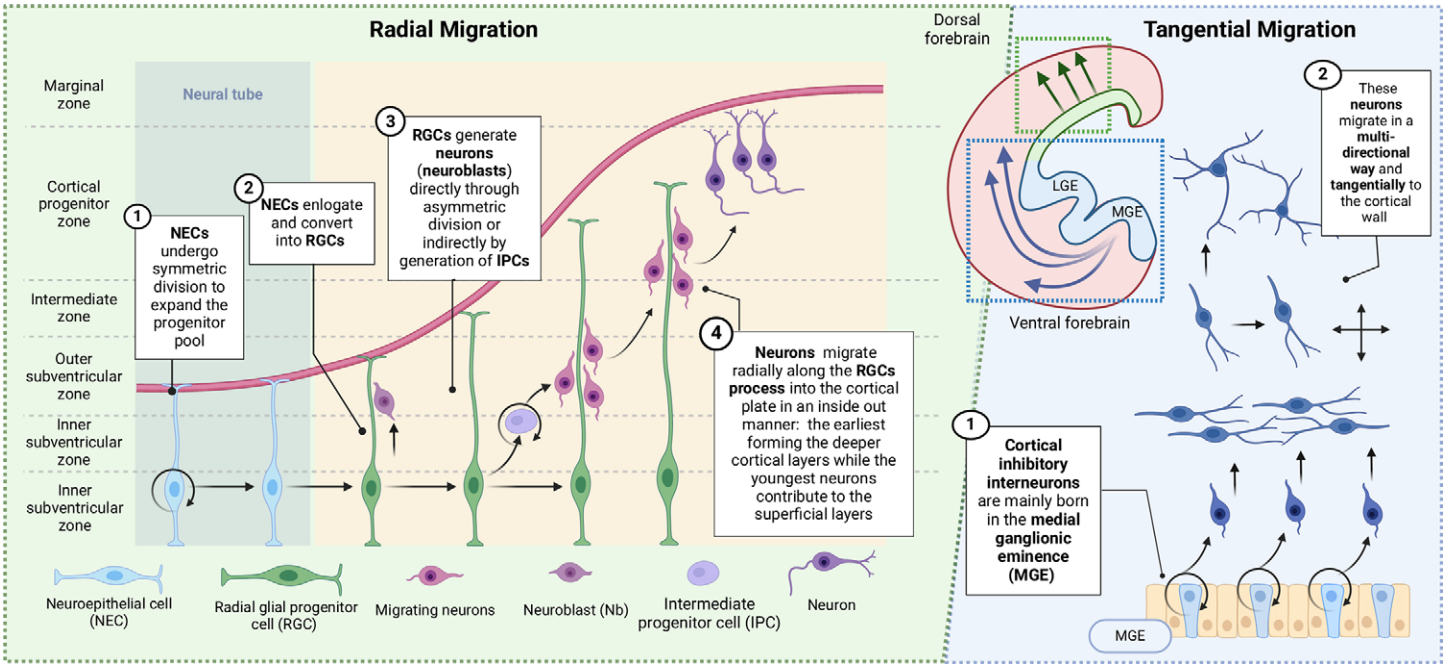

Figure 2. Schematic diagram describes and illustrates two modes of neuronal migration in the developing brain (2). In radial migration, excitatory pyramidal projection neurons move from the ventricular zone to the cortical plate, using radial glial cells as their scaffolds. In this way, cortical layers are formed in an inside-out manner, with later-born neurons acquiring positions in the upper cortical layers. In tangential migration, inhibitory interneurons originate from distinct proliferative zones, such as the medial ganglionic eminence in the ventral brain. These interneurons migrate in multiple streams into the cerebral wall when reaching appropriate positions in the neocortex. *LGE* = lateral ganglionic eminence. (Created with BioRender.com.)

paleocortex is intermediate in phylogenetic origin (eg, cingulated gyrus); and archicortex is the oldest in phylogenetic origin and is comprised of only three layers. The areas of cortices between the archi-, paleo-, and neocortex show a gradual transition of cytoarchitecture that can be described with the suffix "peri" (8). Interestingly, the embryologically older archi- and paleocortex have somewhat higher signal intensity on T2-weighted, diffusion-weighted, and fluid-attenuated inversion-recovery (FLAIR) images; these physiologic regional signal intensity changes can be seen in healthy adults and children and are well seen at 3-T MRI (9).

The most important imaging method for assessment of MCD is unquestionably MRI. Radiologists should advocate the use of 3 T instead of 1.5 T and use the highest resolution and greatest contrast scanner and sequences available. When cortical anomalies are detected at imaging, the effects of age on the myelination process must be considered. MCD can be more easily identified before myelination has begun or after it is completed (ie, the 3rd year of life). The scheme depicted in Figure 3 summarizes these properties for age and MRI sequences. In addition, it is important to remember that the gyrus and sulcus may have an immature appearance in cases of extreme prematurity. Complex interactions between cortical surface area and brain size promote changes in depth, gyrification, volume, and curvature as newborns become older (10).

A normal cortex at MRI should have these imaging features: *(a)* a normal external cortical surface and a smooth and sharply delineated cortico-subcortical junction and *(b)* sulci that may have slight anatomic variations but are uniform and symmetric in their position and depth. Cortical measurements obtained at brain MRI should not be strictly regarded as cutoff values, as a variety of factors can affect cortical thickness, including age, head size, sex, and any sequelae (9).

New Consensus: Basic Introduction

The first MCD classification was proposed in 1996 by Barkovich et al (11), based on the concept of interruption of the three major stages of cortical development: cell proliferation, neuronal migration, and postmigrational cortical organization. It was revised in subsequent years (2001, 2005, and 2012) by Barkovich et al, aided by the increasing accessibility and resolution of MRI technology, new knowledge of embryologic processes, and recent discoveries of genetic and pathologic mechanisms. The current categorization is shown in Table 1 (9) and is more comprehensively detailed in Table S1.

Classifications of MCD continue to evolve as new knowledge emerges. At the same time, the heterogeneity of phenotypes and vast genetic backgrounds add complexity to frame this variety of disorders in tight definitions. Agreement and use of a common language among different professionals, from research to clinical practice, are necessary steps to achieve greater advances by improving genotype-phenotype correlation and allowing genetic tests to be better targeted (9).

The European Network Neuro-MIG on brain malformations published a consensus document in 2020 that provides recommendations to assist expert and nonexpert clinicians in the MCD diagnostic workup (12). Practice guidelines for MCD radiologic diagnosis were also conceived (9), and considerations regarding definitions and classifica-

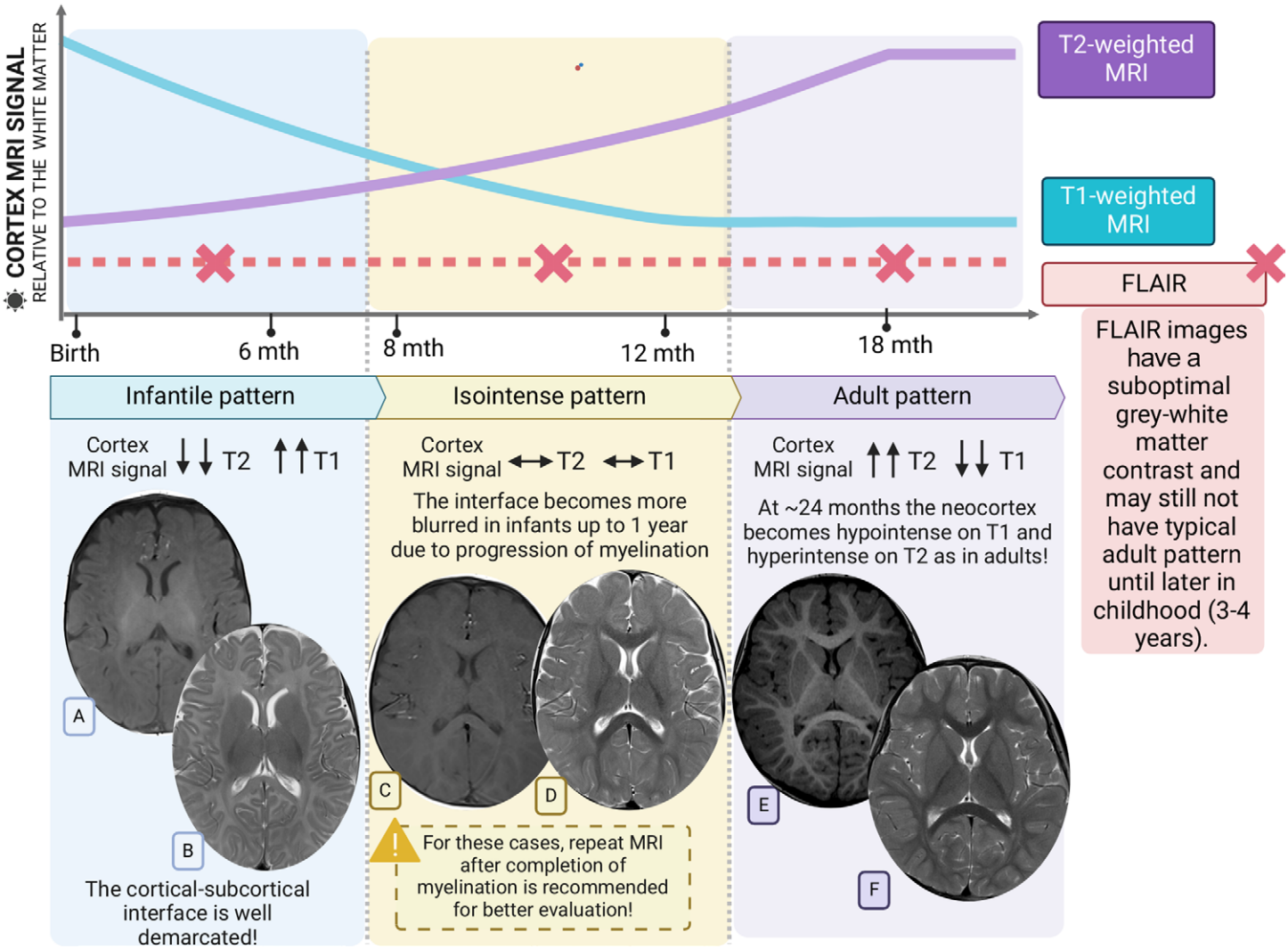

Figure 3. Accurate identification of malformations requires an understanding of the neocortex's imaging aspects, considering age and myelination status. In neonates and infants up to 6 months of age, the cortex displays hyperintensity at T1-weighted MRI *(A)* and hypointensity at T2-weighted MRI *(B)*, known as infantile pattern. The cortical-subcortical interface is clearly defined in the neonatal period *(B)* but becomes progressively blurred *(C, D)* in infants up to 1 year of age due to ongoing myelination, referred to as the isointense pattern. This phenomenon, particularly between 8 and 12 months of age, underscores the importance for radiologists to recommend repeat MRI after complete brain myelination for a more precise assessment. With advancing myelination, the neocortex at 24 months of age is hypointense at T1-weighted MRI *(E)* and hyperintense at T2-weighted MRI *(F)*, manifesting in the same manner as the adult pattern. *mth* = month. (Created with BioRender.com.)

tion were made based on new evidence. The main modifications comprise more assertiveness in describing key terms, as detailed further in each section, and the understanding that developmental stages are genetically and functionally interdependent at the expense of rigid sorting systems. Perhaps the most relevant insight concerns acknowledgment of the multifactorial nature of what is described as PMG, suggesting reallocation or coexistence of this pattern in the group of late migrational disorders, as well as its resemblance at imaging to cobblestone malformation, which will likely compose a recognized spectrum of cobblestone or PMG-like because the pathophysiologic circumstances seem to be shared. Other considerations embrace the concepts of focal cortical dysplasia (FCD) type III, subcortical band heterotopia (SBH), and LIS severity. The fundamental changes are listed in Table 2 (9).

Malformations of Cortical Development

In the following sections, the different types of MCD and their definitions, classification, imaging patterns, and genetic characteristics are discussed. At the end of the article, the authors propose a flowchart for the imaging approach to MCD.

Group 1: Abnormal Cell Proliferation or Apoptosis

Reduced Proliferation or Increased Apoptosis: Microcephaly

Microcephaly is usually defined as an occipitofrontal circumference equal to or more than 2 SDs below the mean for age, sex, and population (13,14). With a few exceptions (eg, some craniosynostosis), a small head (microcephaly) also implies a small brain (microencephaly).

Table 1: Current Categorization of MCD

Group 1: abnormal cell proliferation or apoptosis
Primary microcephaly
Brain overgrowth spectrum
Megalencephaly
Hemimegalencephaly
FCD type IIa
FCD type IIb or cortical tubers
Group 2: abnormal neuronal migration
Heterotopia
LIS
Agyria or pachygyria spectrum and SBH
LIS type I
Cobblestone (LIS type II)
PMG
Schizencephaly
Group 3: abnormal postmigrational development
Dysgyria
FCD type I
FCD type III
Secondary microcephaly

Source.—Reference 9.
Note.—FCD = focal cortical dysplasia, SBH = subcortical band heterotopia.

Most children with an occipitofrontal circumference between 2 and 3 SDs below the mean (mild microcephaly) have normal cognition. However, the chances of intellectual disability increase markedly for children with an occipitofrontal circumference of 3 or more SDs below normal (severe microcephaly) (15).

Microcephaly can be classified as primary (congenital) or secondary (postnatal). This distinction is essential for etiologic investigation and prognostic definition. Both types of microcephaly can be genetic or acquired. Additionally, microcephaly can manifest as an isolated finding (nonsyndromic) or with additional features (syndromic), such as cardiovascular disease (eg, Williams syndrome), facial dysmorphism and limb anomalies (eg, Cornelia de Lange syndrome), short stature (eg, Seckel syndrome), or radiosensitivity (eg, Bloom syndrome).

Imaging studies of patients with microcephaly primary hereditary traditionally show normal or simplified cortical gyral patterns, without severe malformations (Fig 4). A *simplified gyral pattern* is defined as a reduced number of gyri with shallow sulci (one-quarter to one-half of normal depth) but with normal thickness of the cerebral cortex at brain MRI (9). Adachi et al (16) found a strong correlation between the degree of microcephaly and the presence of a simplified gyral pattern. Nevertheless, the growing number of reported microcephaly primary hereditary–linked mutations (Table 3) suggests that other brain architecture abnormalities could develop (17–19).

In contrast, secondary microcephaly most frequently results from disruptions in postmigrational development. This topic is included here for didactic purposes. In addition to brain malformations, genetic metabolic disorders and multiple environmental factors must be investigated, including central nervous system infections, drug or toxin exposure, trauma, hypoxic-ischemic insults, intraventricular hemorrhages, severe malnutrition, and systemic diseases.

Among the central nervous system infections, microcephaly stands out in Zika virus infection. The collapsed skull appearance and cortical-subcortical junction calcifications may also favor this cause in endemic areas over the classic infectious causes (TORCH syndrome) (20) (Fig 5).

Enhanced Proliferation or Reduced Apoptosis: Brain Overgrowth Spectrum

Megalencephaly results from increased proliferation or decreased apoptosis and may have a normal-appearing cortex or may be associated with cortical malformations (also known as dysplastic megalencephaly) and/or white matter signal intensity abnormalities (21). It has been recently demonstrated that certain types of dysplastic megalencephaly are vast regions of localized cortical dysplasia type II (see the next section), with the area size determined by the time and extent of the underlying mutation (22).

It is important to differentiate megalencephaly from macrocephaly. *Macrocephaly* (or macrocrania) is defined as an occipitofrontal circumference equal to or more than 2 SDs above the mean, whereas megalencephaly refers to a primarily developmental brain disorder associated with an abnormally large brain size (21). Macrocephaly has a wide variety of causes besides megalencephaly, including hydrocephalus and increased skull thickness. Mild macrocephaly with an otherwise structurally normal brain can be seen in typically developing children, often in the setting of benign enlargement of the subarachnoid spaces in infancy (23) (Fig 6). Megalencephaly can result from abnormalities in signaling pathways that control brain cell growth, differentiation, cell cycle regulation, and survival (developmental megalencephaly) or from certain metabolic disorders and leukodystrophies (metabolic megalencephaly) (24).

Brain overgrowth can occur bilaterally or unilaterally, with total or partial hemispheric involvement in both scenarios. Unilateral megalencephaly is associated with a lateral ventricle that increases on the affected side; on the other hand, expansile or infiltrative lesions with mass effect compress the ventricular system. *Hemimegalencephaly* (HMEG) is defined as complete unilateral megalencephaly that affects one entire or almost an entire brain hemisphere (25). Focal megalencephaly, which involves up to three cerebral lobes, has been referred to as quadrantic dysplasia, lobar HMEG, or hemi-HMEG and typically affects the frontal lobe or the parieto-occipital lobes (9) (Fig 7).

Although rare, posterior cerebral fossa features may be implicated in the megalencephaly spectrum. During the first 2 years of life, cerebellar expansion (with or without cerebellar cortical dysplasia) sometimes occurs faster than growth of the cerebrum, which can lead to development of cerebellar tonsillar ectopia (26).

Megalencephaly can be isolated or a part of syndromic conditions, such as macrocephaly capillary malformation and megalencephaly PMG–polydactyly hydrocephalus syndromes, epidermal nevus syndrome, congenital lipomatous overgrowth, vascular malformations, epidermal nevus,

Table 2: Novel Considerations regarding MCD

MCD	Former Concept	Novel Considerations
PMG	Classified as a postmigrational disorder	Should be reclassified as a late migrational disorder
Cobblestone or PMG-like cortex	...	New suggested umbrella term to describe overlapping imaging features, considering their same pathophysiologic mechanism
Cobblestone malformation	Classified as LIS type II	Now classified as a distinct entity as it is an overmigration rather than undermigration disorder
FCD type III	Classified separately from FCD types I and II	Might be not maintained as a separate entity
SBH (double cortex syndrome)	Same classification as other heterotopias	Now recognized as part of the LIS spectrum
LIS	Subdivided in classic LIS (LIS type I) and variant LIS	Best described based on the severity and gradient of the gyral malformation, cortical thickness, and associated brain malformations
Dysgyria	...	New term to describe a dysmorphic cortex

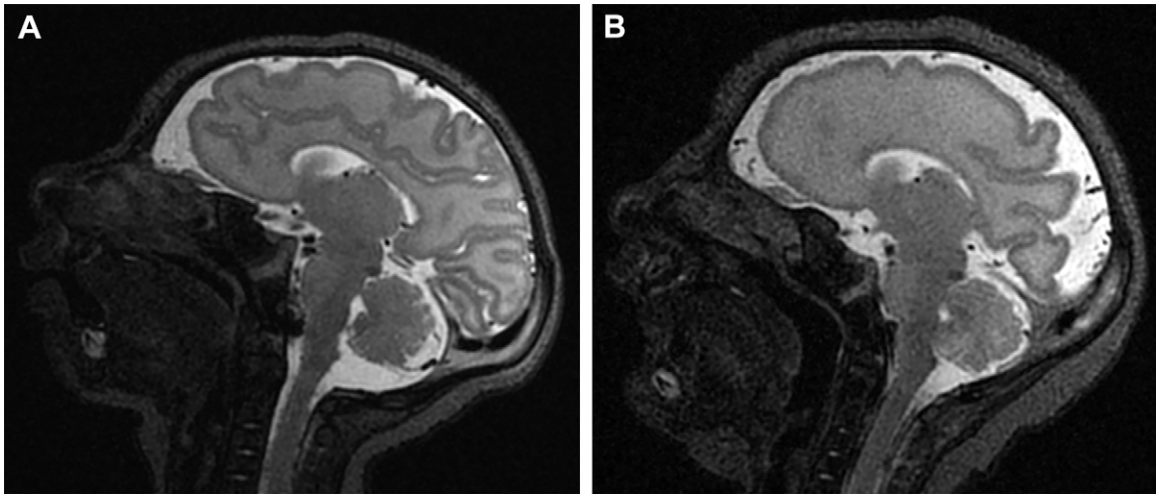

Figure 4. Microcephaly in two infants. Sagittal T1-weighted MR images show a normal gyral pattern **(A)** and a simplified gyral pattern **(B)**.

Table 3: Genetic Causes of Primary Microcephaly

Findings at Presentation	Associated Gene Mutation
Microcephaly primary hereditary (nonsyndromic)	*ASPM* (*MCPH5*) and *WDR62* (*MCPH2*) gene mutation
Profound microcephaly, very simplified gyral pattern, periventricular nodular heterotopia, and a very small brainstem and cerebellum	*NDE1* gene mutation
Mild microcephaly with bilateral periventricular heterotopia and putaminal hyperintensity	*ARFGEF2* gene mutation
Wrapping of the frontal horns around the outside of the basal ganglia, absence of the anterior limb of the internal capsule, profound microcephaly, LIS, absent or very small corpus callosum, and marked cerebellar hypoplasia with large tectum	*TUBA1A* gene mutation
Postnatal microcephaly with disproportionate brainstem and cerebellar hypoplasia and reduced frontal gyri volume; normal-sized corpus callosum may give an impression of callosal thickening	*CASK* gene mutation

spinal and skeletal anomalies, scoliosis syndrome, and others (9). These diseases often involve increased growth of the body and specific cutaneous hallmarks, including cutaneous nevus, as a result of neural crest participation in postzygotic somatic mosaicism (26). An increasing number of defects in genes involved in cell growth and proliferation pathways are being identified in megalencephaly and are detailed in Table 4 (27–29).

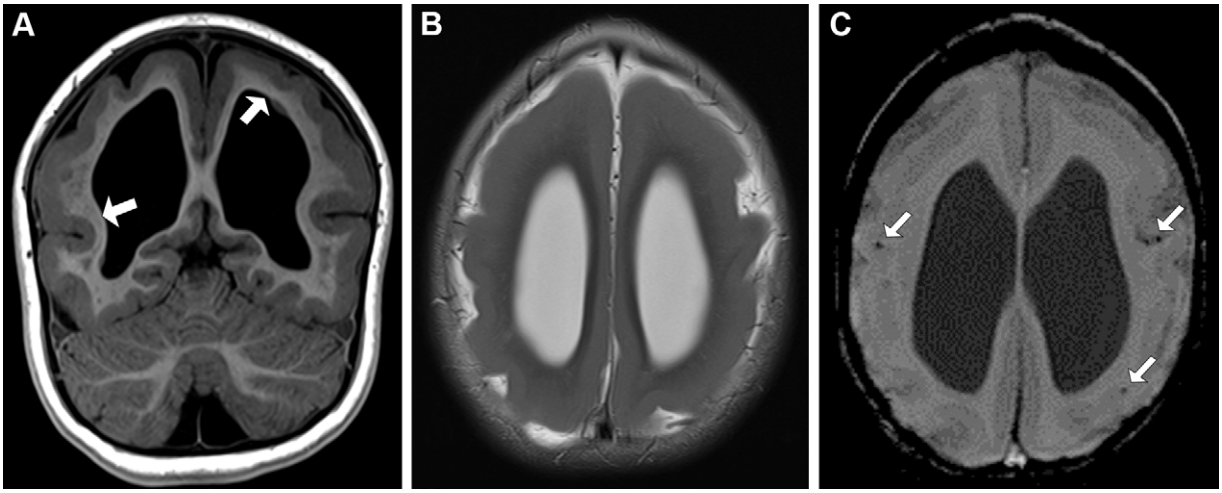

Figure 5. Zika virus microcephaly in a 2-year-old boy. **(A, B)** Coronal T1-weighted **(A)** and axial T2-weighted **(B)** MR images show cortical thickening and LIS pattern characterized by frontal agyria and bilateral temporoparietal pachygyria. There are small foci of subependymal nodular gray matter heterotopia (arrows in **A**) in the walls of the body of the left lateral ventricle and the atrium of the right lateral ventricle. **(C)** Axial susceptibility-weighted MR image shows small foci of calcifications diffusely distributed in the subcortical regions of the brain parenchyma (arrows).

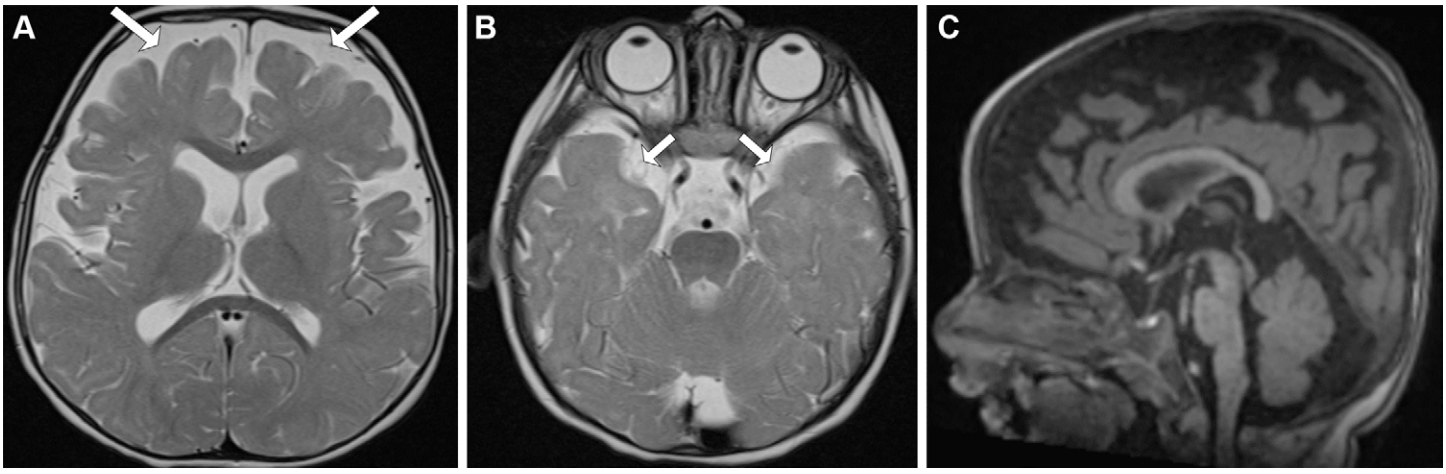

Figure 6. Benign external hydrocephalus in an 8-month-old boy undergoing macrocrania investigation. **(A, B)** Axial T2-weighted MR images show enlargement of cerebrospinal fluid spaces (arrows), especially in the frontal lobes and temporal poles. **(C)** Sagittal T1-weighted MR image shows an increased skull-to-face ratio.

Abnormal Proliferation: FCD Types IIA and IIB or Cortical Tubers

FCD is a heterogeneous group of focal abnormalities of cerebral cortex cytoarchitecture, with diverse histologic appearances. FCD manifests as disordered cortical lamination, cytoarchitectural lesions, and underlying white matter abnormalities (30). It is highly associated with medically intractable epilepsy; in fact, it was the most common diagnosis in a sample of 9523 children who underwent epilepsy surgery for drug-resistant seizures (31).

FCD is classified into three neuropathologic subgroups by the International League Against Epilepsy (32) based on the severity of cytoarchitectural disruption and the abnormal cell types found. Nevertheless, there has been some controversy about this classification, possibly with a future new classification system (33).

FCD Type I.—FCD type I consists of abnormal cortical layering and has three subtypes. In FCD type Ia, there is failure in the correct radial migration of neurons, which is the path that neuronal progenitors take through the radial-oriented glial cells. In FCD type Ib, there is a derangement of the six-layered tangential composition of the neocortex; and in FCD type Ic, both processes occur. All three variants can show heterotopic neurons in white matter and hypertrophic neurons (outside layer 5), as well as normal neurons with abnormal dendrites. They may affect one or multiple lobes (34).

FCD type I is radiologically and pathologically challenging to diagnose and still lacks specific molecular and genetic biomarkers, although genetic alterations of *DEPDC5*, *AKT3*, *KCNT1*, *NPRL2*, *NPRL3*, *PCDH19*, *SCN1A*, *SLC35A2*, and *STXBP1* have been described (35). MRI may show abnormal signal intensity of the subcortical white matter, with blurring of the

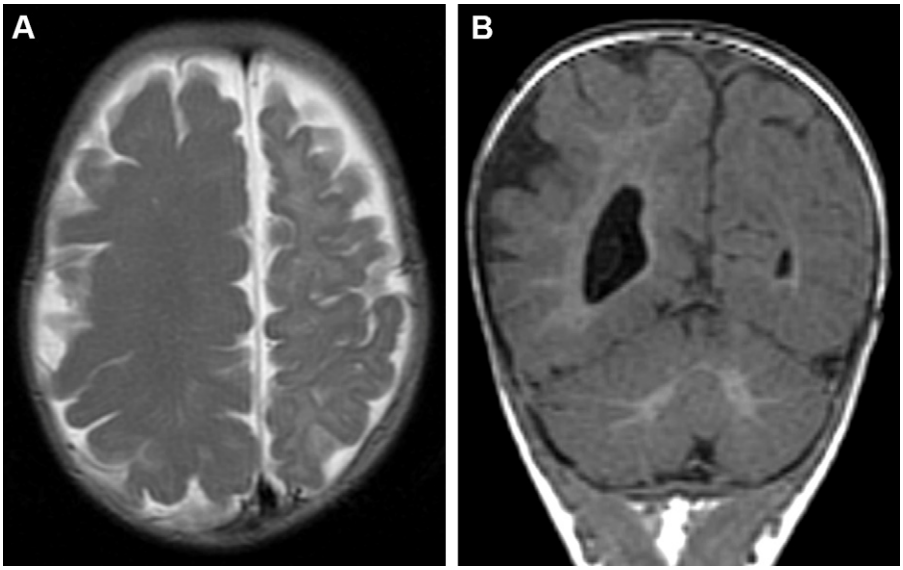

Figure 7. Hemimegalencephaly in a 3-week-old newborn. Axial T2-weighted **(A)** and coronal T1-weighted **(B)** MR images show a marked volumetric increase of the right cerebral hemisphere. Note the enlarged ventricle **(B)** and accelerated myelination **(A)** in the affected side.

Table 4: Gene Defects Identified and Associated with Megalencephaly

Gene mutation
PI3K–AKT–mTOR pathway
RAS–MAPK–ERK pathway
DNA methyltransferase
Transcription initiation regulators and tyrosine kinase receptor
Other findings
Isolated or syndromic megalencephaly, with somatic (body) overgrowth and/or other MCD, including PMG

gray-white matter junction and prominent segmental or lobar hypoplasia of the affected region (36). Asymmetric lack of subcortical myelination is a rather specific finding for FCD type Ia (17).

FCD Type II.—FCD type II manifests as a marked disruption of cortical lamination with morphologically abnormal cell types, notably dysmorphic and cytomegalic neurons. It is divided according to the absence (IIa) or presence (IIb) of balloon cells, which are unusual large cells with abundant opalescent eosinophilic cytoplasm and one or more eccentric nuclei. FCD type II and dysplastic megalencephaly form a spectrum of disorders in the mTOR pathway and its activators (*AKT3*, *PIK3CA*, and *RHEB*), as well as in its repressors (*DEPDC5*, *TSC1*, and *TSC2*) (36).

The tuberous sclerosis complex (TSC) tubers can be considered an FCD type IIb, although it is not classified as such by the International League Against Epilepsy. TSC and FCD type IIb lesions are histologically similar, and the cause of both conditions involves the mTOR pathway genes *TSC1* and *TSC2*. Furthermore, patients with panel-negative FCD type II have significant pS6 immunostaining, indicating that all FCD type II entities are mTORopathies (37).

FCD type II is usually identified at MRI. Relevant imaging findings include abnormal cortical thickness, gray-white matter junction blurring, cortical and subcortical signal intensity abnormalities, and aberrant gyral and sulcal patterns. On T2-weighted and FLAIR images (Fig 8), the transmantle sign appears as radially oriented and funnel-shaped high signal intensity in the subcortical white matter that points to the ipsilateral ventricle and is highly specific for FCD type IIb, including the tubers of TSC. Also, hypointense bands at the portico-subcortical junction have been reported on 7-T susceptibility-weighted images (38). Calcifications may occasionally be seen, especially in tubers.

Imaging patterns vary significantly depending on the myelination stage. In unmyelinated brains, FCD often manifests as T2-hypointense and T1-hyperintense lesions (39) (Fig 9). As myelination advances, FCD lesions become more similar to the surrounding brain parenchyma, making identification more difficult.

The differential diagnosis comprises low-grade tumors, particularly glioneuronal tumors such as gangliogliomas, as well as new histologic causes such as “oligodendrocytosis” (40) and “mild malformation of cortical development with oligodendroglial hyperplasia” (41), characterized on MR images by abnormal signal intensity within the anatomic region of seizure onset. Although coexisting FCD and low-grade tumors are a recognizable entity, some aspects that may help to differentiate these pathologic conditions are patient age at epilepsy onset (younger age in patients with FCD) and loss of *N*-acetylaspartate and increase of choline at proton MR spectroscopy, which are more pronounced in low-grade gliomas than in FCD (42).

FCD Type III.—FCD type III has architectural distortion of cortical layers around an epileptogenic lesion, such as a tumor or a vascular malformation. Molecular and clinical biomarkers are needed for diagnosis, and FCD type III might not be maintained as a separate entity in the upcoming revised classification (43). It is divided into four subtypes according to the location of the affected cortex: type IIIa, in the

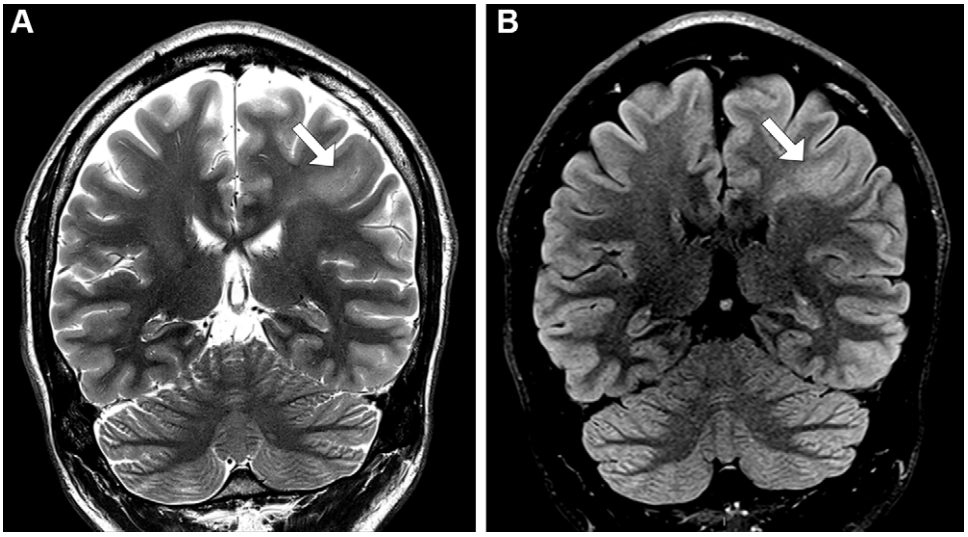

Figure 8. FCD type II with transmantle sign in a young man. Coronal T2-weighted **(A)** and FLAIR **(B)** MR images demonstrate abnormal cortical thickening, associated with loss of white-gray matter differentiation (arrow in **A**) and hyperintensity in the cortical and subcortical areas of the left frontal lobe (arrow in **B**).

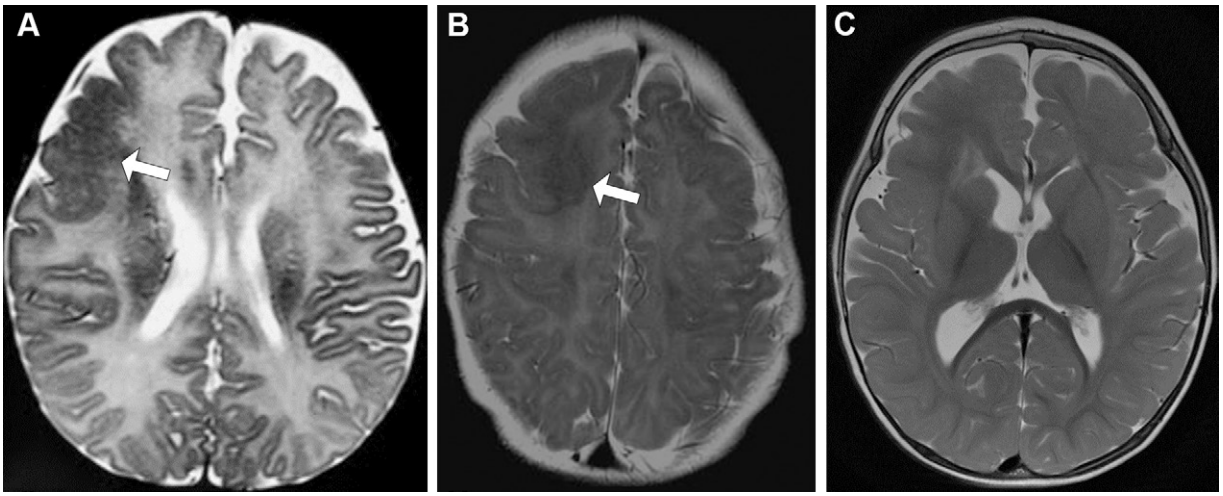

Figure 9. Changing appearance of FCD type II in an infant. **(A, B)** Axial T2-weighted images show an infantile cortical pattern at age 2 months **(A)** and 6 months **(B)**, with cortical thickness and adjacent white matter hypointensity (arrow). The right frontal lobe (arrow) also has blurring of the white-gray matter junction and accelerated myelination. **(C)** Axial T2-weighted MR image at 12 months of age shows that in the transition to the adult cortical pattern, FCD changes become more challenging to identify due to the similar signal intensity between white and gray matter.

temporal lobe with hippocampal atrophy; type IIIb, adjacent to a glial or glioneuronal tumor; type IIIc, adjacent to a vascular malformation; and type IIId, adjacent to other lesions that form in early childhood (Fig 10).

If FCD is suspected, it is recommended to review MR examinations in search of eventually overlooked lesions (33). Multiplanar and three-dimensional reconstructions may aid in their detection, and artificial intelligence is another promising tool to be incorporated in this diagnostic workup (9,35).

Group 2: Abnormal Neuronal Migration

Decreased Migration

Heterotopia

Gray matter heterotopia consists of clusters of healthy neurons in abnormal positions, mostly caused by defective migration (44).

Periventricular Nodular Heterotopia.—Periventricular nodular heterotopia is the most common type of heterotopia. It is usually composed of nodules of gray matter that line the ventricular wall. These nodules can range widely in number, location, size, and sometimes shape, and they can be associated with a variety of other brain or systemic malformations (9,45). Small nodules of gray matter can be seen close to the ependymal layer, elevating it and distorting the ventricle outlines. They are most frequently observed in the trigones and occipital horns regions (9,46).

On all MR images, gray matter heterotopias are isointense to the cerebral cortex (Fig 11). This is valid regardless of the location of the heterotopia (9,45).

It is important to distinguish between periventricular nodular heterotopia and tuberous sclerosis subependymal nodules. The latter are positioned perpendicular to the ventricular walls, are not isointense to gray matter, frequently calcify, and may have enhancement after contrast agent administration (9,45,46).

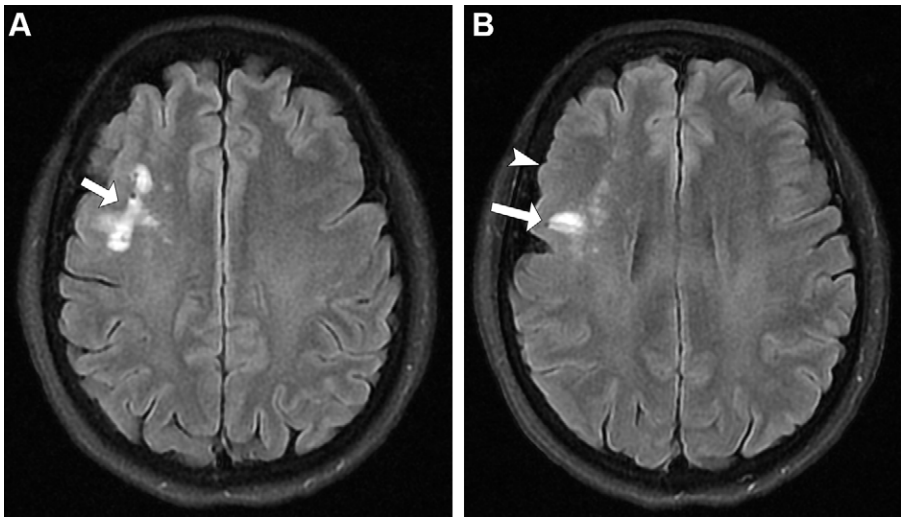

Figure 10. FCD type III with anomaly of venous development in a 12-year-old girl. Axial FLAIR MR images show cortical thickening with changes in the gyration and sulcation pattern (arrowhead in **B**), as well as irregularities and blurring of the white-gray matter junction, affecting the right frontal lobe. The area of hyperintensity in the adjacent subcortical white matter (arrow) has internal vascular structures of probable venous origin that extend to the semioval center and the ependymal surface of the right lateral ventricle.

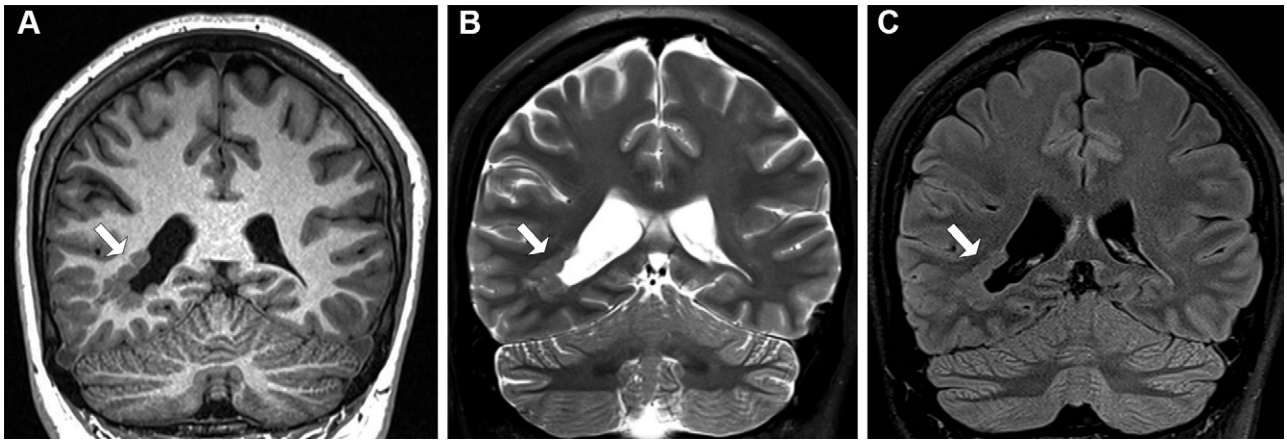

Figure 11. Coronal T1-weighted **(A)**, T2-weighted **(B)**, and FLAIR **(C)** MR images in an 8-year-old girl with developmental delay show subventricular heterotopia (arrow). The nodules have a similar signal intensity to that of gray matter with all sequences.

The filamin A protein encoded by the *FLNA* gene at Xq28 is known to interact with more than 90 other proteins, some of which may be involved in neuronal migration, and is an recognizable underlying genetic cause related to periventricular nodular heterotopia (PVNH) (47). The imaging pattern that should raise suspicion for *FLNA* mutation is bilateral and symmetric PVNH, with a slight preference for the frontal horns and ventricular bodies. *FLNA* mutation is also associated with cardiac malformations. Other genes including *MAP1B*, *TMTC3*, *MEN1*, *NEDD4 L*, *ACTG1*, and *ARFGEF2* have been linked to *FLNA*-negative PVNH (48).

***Subcortical Heterotopia.*—**Subcortical heterotopia (SUBH) is a grouping of neurons in the white matter of the cerebral hemispheres. It usually extends from the ventricular surface to the overlying cortex, which is commonly dysplastic and lacks well-defined intervening white matter (Fig 12) (9,49). There is an association between SUBH and LIS (discussed in the next section) related to some genetic mutations such as *TUBG1*, *TUBA1A*, and *APC2*. Other genes associated with SUBH are *COL4A* (brain small vessel disease), *GPSM2* (Chudley-McCullough syndrome), and *POMT2* (dystroglycanopathy) (50).

A narrow but distinct band or wedge of gray matter that extends perpendicularly from the ependyma to the cortex is referred to as transmantle columnar heterotopia. At imaging, transmantle heterotopia may involve an entire cerebral lobe, manifesting as a remarkable "lobe within a lobe" appearance; this is known as sublobar dysplasia (1,9).

Lissencephaly

LIS is characterized by a smooth brain surface with wide or missing gyri or convolutions, an unusually thick cortex, and histopathologic signs of aberrant cortical anatomy (9). It is caused by disturbed neuronal migration during early stages of cortical development. The spectrum of LIS encompasses *agyria* (Fig 13), defined as cortical regions with sulci more than 3 cm apart; *pachygyria,* defined as abnormally wide gyri with sulci 1.5–3 cm apart; and *SBH,* defined as gray matter longitudinal bands located deep in the cerebral cortex and separated from it by a thin layer of white matter, hence the term *double cortex syndrome* (51,52) (Fig 14).

The distinguishing imaging feature of LIS is a thick cerebral cortex with decreased gyration. In agyria, the brain exhibits a figure-of-eight form due to a complete lack of sulci, and broad, vertically oriented sylvian fissures. In pachygyria,

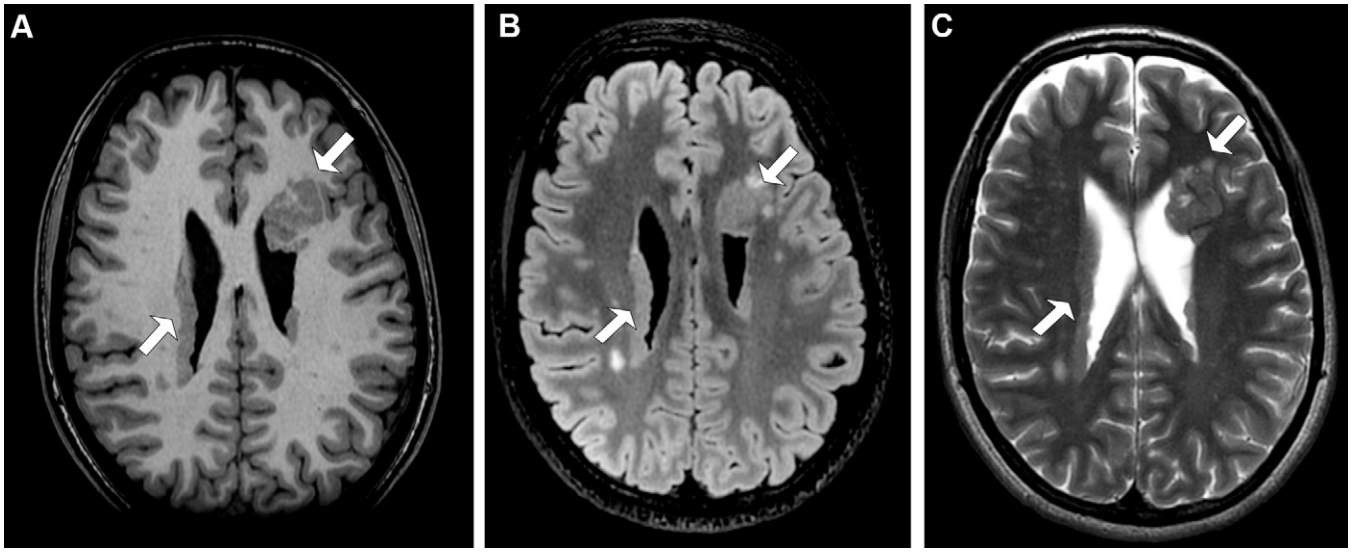

Figure 12. Bilateral nodular periventricular and left subcortical heterotopia (adjacent to the left frontal horn of the lateral ventricle) in a male infant. Axial T1-weighted **(A)**, FLAIR **(B)**, and T2-weighted **(C)** MR images show tissue along the ependymal surface of the lateral ventricles (arrows) with similar signal intensity to that of the cortex with all sequences, corresponding to nonmigrated neuronal tissue.

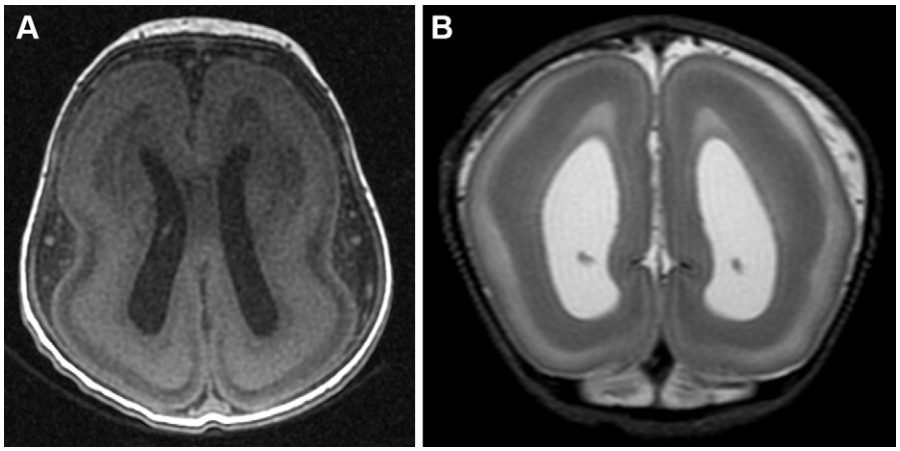

Figure 13. Agyria in a 5-year-old girl. Axial T1-weighted **(A)** and coronal T2-weighted **(B)** MR images show diffuse cortical thickening with an absence of sulci and gyri. The supratentorial brain assumes a figure 8 shape.

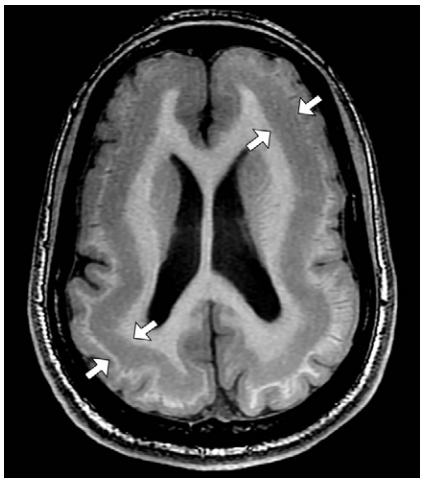

Figure 14. SBH in an infant. Axial T1-weighted MR image demonstrates bilateral bands of heterotopic gray matter interposed between the lateral ventricles and the cortical mantle.

the cortex is more frequently divided into broad, coarse gyri by at least a few shallow sulci (9) (Fig 15).

LIS can be classified by cortical thickness as classic LIS or thick LIS when the cortex is 10–15-mm thick; thin LIS when the cortex is 5–10-mm thick; and variable LIS when there are coexisting areas of thick and thin LIS (51,52). At imaging, LIS is better classified based on the severity (grade) of gyral abnormality, anterior-posterior gradient, cortical thickness, and eventually associated brain malformations. The severity is divided into diffuse or partial for LIS and SBH, and *gradient* refers to the predominant topography of the anomaly (anterior, posterior, or no gradient). The cortical thickness and appearance involve "simplified gyration overlying SBH," "thin undulating," "thin variable dysgyria," "thin with enlarged lateral ventricles," "thin mantle," or "thick classic." Noncortical brain malformations include basal ganglia dysgenesis, corpus callosum dysgenesis, tectal hyperplasia, brainstem hypoplasia, and cerebellar dysgenesis or hypoplasia (diffuse or vermian) (51–53). Many different gene mutations have been identified in LIS, as depicted in Table 5 (52–54) (Fig 16).

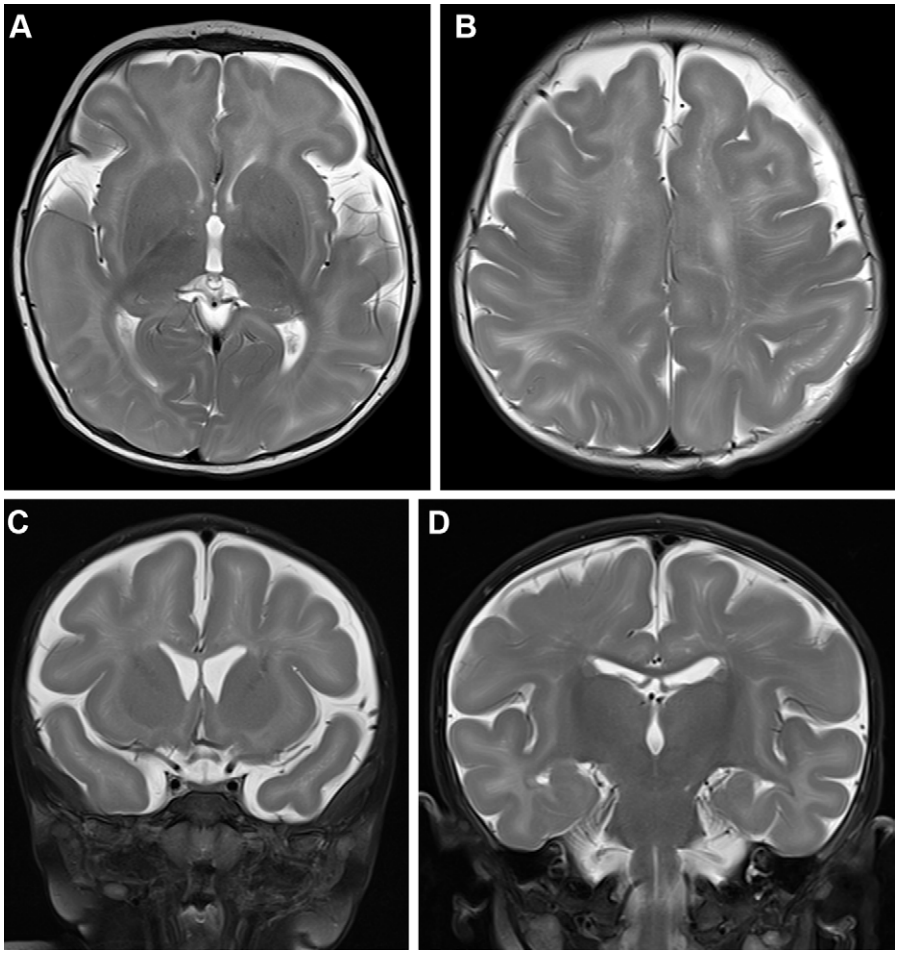

Figure 15. Pachygyria in a 4-month-old infant. Axial **(A, B)** and coronal **(C, D)** T2-weighted MR images show simplification of the sulcation and gyration pattern that is associated with diffuse cortical thickening and subtle blurring of the white-gray matter junction (bilateral and symmetric) more evident in the temporal poles and frontal and parietal lobes.

Table 5: Main Genes Associated with LIS

Gene Abnormality	Associated Phenotype
Mutation or deletion of *LIS1* (*PAFAH1B1*)	Isolated LIS syndrome or Miller-Dieker syndrome (spectrum of LIS with facial dysmorphism)
DCX (doublecortin protein) located in X chromosome	Classic LIS and SBH (affecting males more severely)
ARX	Temporal-predominant LIS variant or X-linked LIS with abnormal genitalia
RELN	LIS associated with cerebellar hypoplasia and hippocampal abnormalities
Tubulinopathy (*TUB*) gene mutation: *TUBA1A*, *TUBB2B*, *TUBB*, *TUBB3*, and *TUBA1A*	LIS with cerebellar hypoplasia, which can be associated with microcephaly or normal head size, thin cortex, or striking *TUB*-dysgyria

Cytomegalovirus has been linked to the emergence of LIS because it affects the developing fetal brain, lowering blood flow. Early infection is more likely to result in LIS, given that neuronal migration occurs early in pregnancy (55) (Fig 17).

Microlissencephaly

Microlissencephaly (MLIS) is the combination of LIS and severe congenital microcephaly. It represents a severe and poorly understood group of cortical abnormalities involving tubulinopathy spectrum, Norman-Robert syndrome with LIS with cerebellar hyperplasia phenotype, and Barth MLIS syndrome, which is the most severe. Pathogenic mutations in the genes *DMRT2*, *NDE1*, *KATNB1*, *RNU4ATAC*, *TUBGCP2*, and *CIT* are linked to severe congenital microcephaly and a greatly simplified gyral pattern, which is particularly pronounced across the frontal lobes. Cerebellar hypoplasia and MLIS frequently coexist (52).

Overmigration

Spectrum PMG and Cobblestone Malformation.—The spectrum of PMG and cobblestone malformation is thought to be due to neuronal overmigration into the leptomeninges through defects in the brain pial surface, with

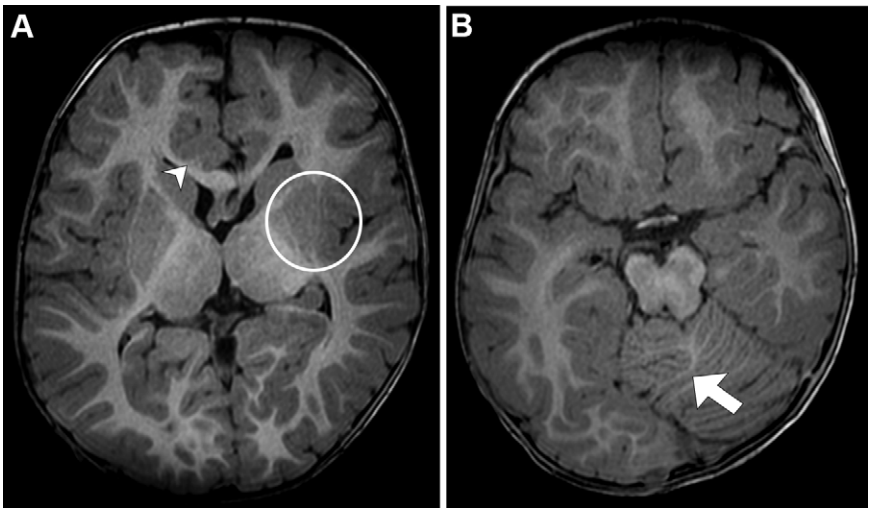

Figure 16. Tubulopathy in a 1-year-old infant with development delay (*TUBB3* gene). Axial T1-weighted MR images demonstrate multifocal areas of gyral thickening and abnormal sulcation in a dysgyric pattern. The interhemispheric falx is hypoplastic, with insinuation of the right frontal parenchyma to the left side (arrowhead in **A**). There are morphologic changes with volumetric reduction of the lentiform nucleus on the left (circle in **A**). Note also the dysmorphic foliation of the cerebellar hemispheres (arrow in **B**).

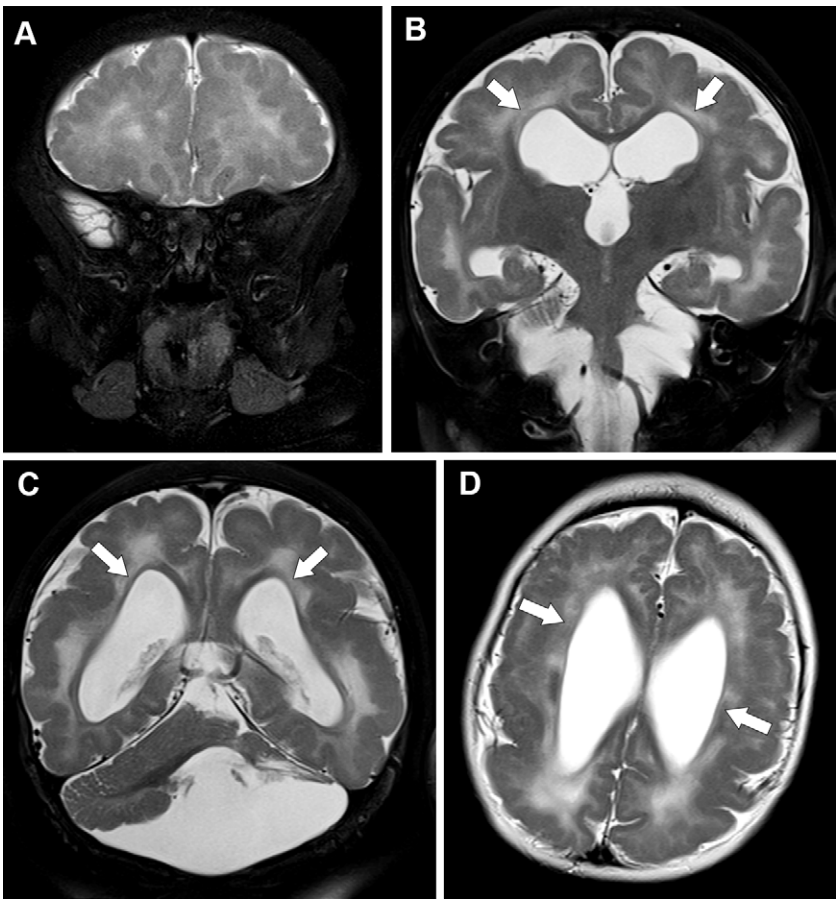

Figure 17. Congenital cytomegalovirus infection in a 6-month-old infant. Coronal **(A–C)** and axial **(D)** T2-weighted MR images show that the ventricular system is dilated (arrows in **B–C**) and the sylvian fissures are elongated. There is diffuse simplification of the cortical gyri with cortical thickening, especially in the lateral temporal and frontoparietal regions, including the perisylvian regions, with a PMG appearance. The left cerebellar hemisphere and cerebellar vermis are atrophic, with encephalomalacia in the superior aspect of the left cerebellar hemisphere and a sequelae appearance. Note also the brainstem volumetric reduction.

leptomeningeal heterotopia (56). As the two entities share the same pathophysiologic mechanism, their imaging features partially overlap, leading to confusion in the reported description and categorization (56). The resulting cortical phenotype will depend on the size of the gaps in the pial limiting membrane and the quantity of neurons that migrate to the subarachnoid space (57). Small gaps that lead to small clumps of neurons on the cortical surface are called PMG, while large gaps leading to relatively smooth layers of neurons on the cortical surface define cobblestone malformation (58) (Fig 18)

At imaging, the appearance can range from an apparently undersulcated brain with a relatively thin cortex to a more convoluted and thicker cortex. In severe cases, a very thick cortex can be misinterpreted as pachygyria (a subtype of LIS) (57). Conversely, apparently smooth cortical surfaces may be due to fusion of the outer cortical (molecular) layer over the microgrooves or even due to technical restrictions, such as suboptimal MRI resolution to identify cortical surface irregularities or a white matter border (59).

Although PMG is still categorized as a postmigrational condition (1), there is mounting evidence that it is primarily

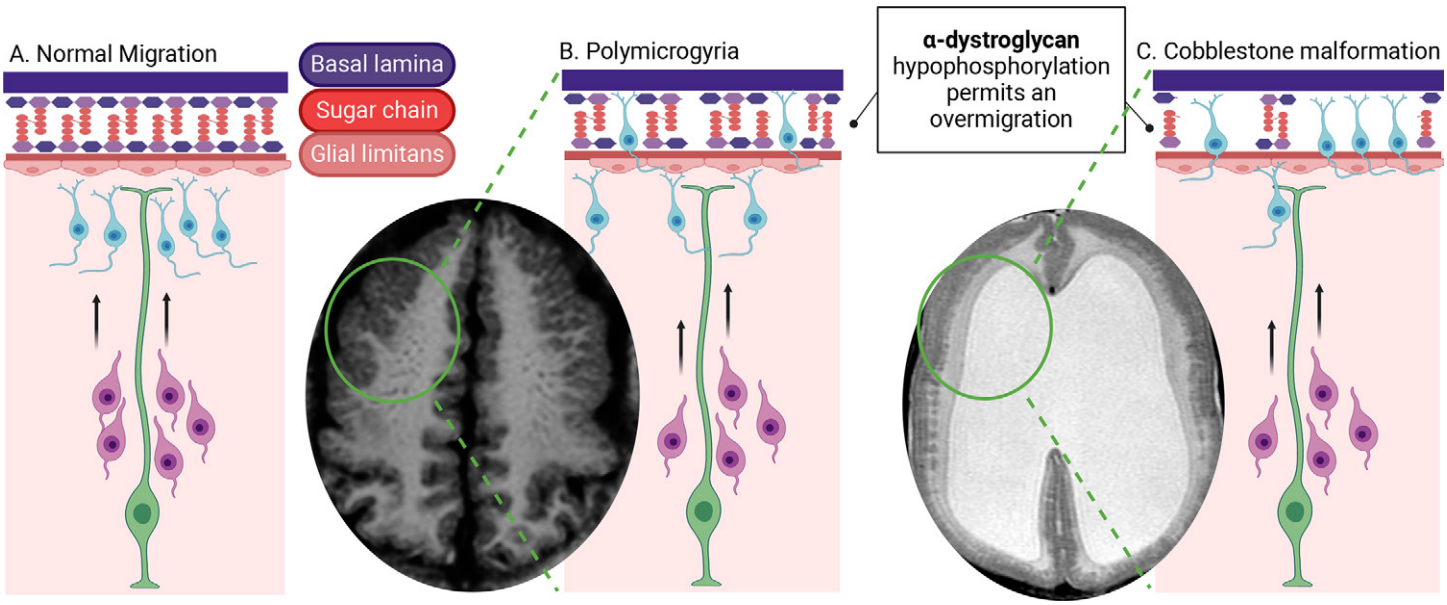

Figure 18. Diagram of hypoglycosylation of α-dystroglycan, which is a transmembrane glycoprotein that binds cells to the extracellular matrix (62). During normal brain formation, α-dystroglycan undergoes glycosylation, providing stability. Left diagram *(A)* illustrates normal glycosylation, maintaining the integrity of the basal lamina and ensuring normal corticogenesis. In contrast, hypoglycosylation of α-dystroglycan leads to gaps in the basal lamina and disorganized overmigration of neurons into the subarachnoid space. Small gaps in the basal lamina contribute to PMG *(B)*, while larger gaps result in the occurrence of cobblestone LIS *(C)*. (Created with BioRender.com.)

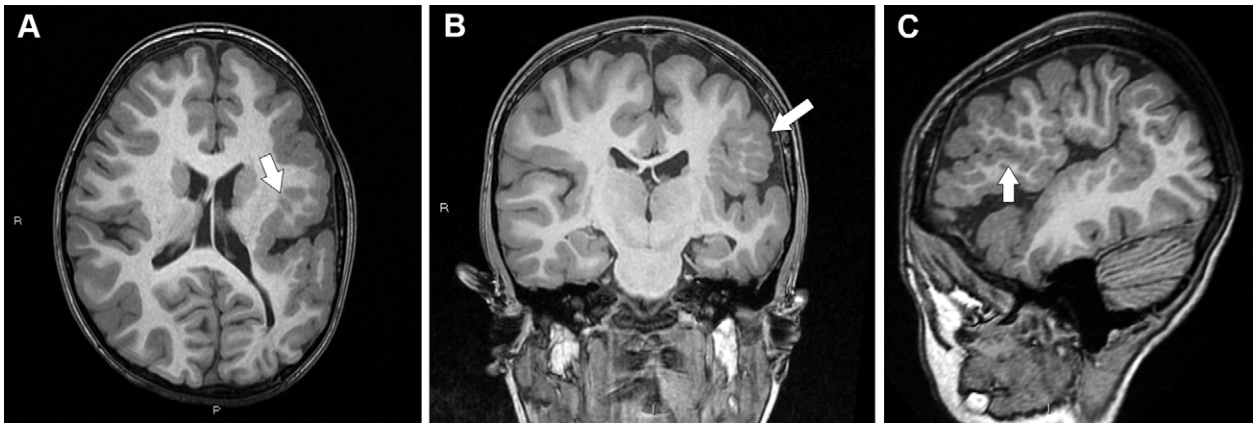

Figure 19. PMG in a 7-year-old girl with closed-lip schizencephaly. Axial **(A)**, coronal **(B)**, and sagittal **(C)** T1-weighted MR images demonstrate cortical thickening with a polymicrogyric appearance (arrow in **B** and **C**) in the left perisylvian region. Note the asymmetry of the cerebral hemispheres, smaller on the left, with a slight increase in the cortical sulci and the lateral ventricle on this side. Also note the verticalization of the sylvian fissures **(C)**.

the result of abnormal late neuronal migration, allowing its reclassification in the group of late migrational (rather than postmigrational) abnormalities (9).

Polymicrogyria.—PMG is characterized by multiple small and compact gyri separated by shallow sulci, resulting in an uneven appearance at the cortical surface and cortical white matter junction. It can result from several gene mutations and copy number variations, as well as nongenetic causes including congenital infections, especially by cytomegalovirus and Zika virus; in utero ischemia; metabolic abnormalities; and exposure to teratogens (9,60). Clinical manifestations vary according to the extent of affected areas, the most common being seizures (78%), global developmental delay (70%), spasticity (51%), and microcephaly (50%) (61).

The topographic distribution of PMG may be focal, multifocal, or diffuse; unilateral or bilateral; and symmetric or asymmetric. The most common sites are the sylvian fissures (60%–70%), notably in the posterior portion, although any part of the cerebral cortex may be affected (9).

At imaging, PMG can be roughly divided into three morphologic subtypes: thick and coarse, fine and delicate, and saw toothed (thin microgyri separated by deep sulci) (Fig 19) (62). Still, the appearance is highly variable and depends on the patient age and degree of myelination, with newborns and infants with an unmyelinated brain having a thin (2–3 mm) and bumpy gray-white junction that commonly changes into a thicker (5–8 mm) and comparatively smoother cortex after myelination is complete (9). Some genetic related syndromes are described in Table 6.

Table 6: Main Characteristics of Cobblestone Malformation related to Dystroglycanopathies

Syndrome	Features
Walker-Warburg syndrome	Cobblestone cortical malformation, fetal hydrocephalus, cerebellar malformation (especially tiny cysts), hypoplastic brainstem with dorsal "kink" at the mesencephalic-pontine junction, retinal dysplasia, agenesis of the corpus callosum, malformations of the eye anterior chamber, Dandy-Walker continuum, cleft lip or palate, posterior encephalocele, ocular colobomas, congenital cataracts, and genital abnormalities
Muscle-eye-brain disease	Cobblestone cortical malformation, retinal detachment with microphthalmia, fetal hydrocephalus, absent septum pellucidum, corpus callosum dysgenesis, and cerebellar malformation (especially inferior vermis hypoplasia)
Fukuyama congenital muscular dystrophy	Temporo-occipital cobblestone cortical malformation, frontal lobe and cerebellar PMG, abnormal signal intensity along the brainstem surface on T2-weighted and FLAIR images, hemorrhage and abnormalities of cerebral superficial and subependymal veins, and hypoplastic brainstem with enlarged collicular plate

Table 7: Mutations Identified in Cobblestone Malformation

Gene Mutations	Findings
POMT1, *POMT2*, *POMGNT1*, *LARGE*, *FKTN*, and *FKRP* mutations	CCM, white matter changes, and cerebellar cysts
TMTC3	CCM and periventricular nodular heterotopia

Note.—CCM = cobblestone cortical malformation.

Cobblestone Malformation.—Cobblestone malformation is characterized by a gross neuroglial overmigration into the subarachnoid space, creating an extracortical layer that results in an agyria appearance, a "cobblestone" brain surface, and enlarged ventricles (63). It used to be referred to as LIS type II (64), but it was eliminated from this group in recognition of its different physiopathologic processes (overmigration rather than undermigration) (58).

A spectrum of autosomal-recessive illnesses with cerebral, ocular, and muscular impairments linked to dystroglycanopathies (congenital muscular dystrophy) are pathognomonic for cobblestone malformation and are described in Table 7 (64–68). The imaging features related to cobblestone malformation are an undersulcated cerebral surface, a mild to moderate thick cortex, and an irregular cortical white matter border that is linked to intracortical white matter with hyperintensity on T2-weighted and FLAIR images and transitory hyperintensity of the underlying white matter (58) (Fig 20). The main mutations are seen in Table 7 (63,68–70).

Abnormal Migration

Schizencephaly.—Schizencephaly is characterized by a cleft lined by polymicrogyric gray matter and/or heterotopia that extends across the full thickness of the cerebral hemisphere, from the ventricular surface (ependyma) to the periphery (pial surface) (9). The etiopathogenesis is unclear, but it seems that the main mechanisms include in utero infections (eg, congenital cytomegalovirus), teratogens, trauma, ischemia, and genetic abnormalities such as *COL4A1, COL4A2*, and tubulins.

Schizencephaly is classified into two morphologic categories and can be unilateral or bilateral. While type I (fused or closed lips) extends from deep brain structures to the surface of the brain without connection to the ventricular system (Fig 21), type II (open or separated lips) connects the ventricular system with the subarachnoid space (Fig 22) (71).

It is frequently associated with other severe brain abnormalities and, in most cases, additional neurologic symptoms. Congenital cytomegalovirus infection can manifest with schizencephaly, white matter lesions, ventriculomegaly, subarachnoid space enlargement, calcifications, and temporal pole cysts. Septo-optic dysplasia may also be associated with schizencephaly (septo-optic dysplasia plus) (72). The use of high-resolution MR images, such as three-dimensional T1-weighted and highly T2-weighted images, is essential to recognize small clefts and ventricular dimples that may indicate the existence of schizencephaly (9).

Group 3: Abnormal Postmigrational Development

Dysgyria

Dysgyria describes a nonspecific malformation in which the cortex has normal thickness but an aberrant gyral pattern, with abnormalities of sulcal depth and orientation (Fig 23). The appearance of the dysmorphic cortex is not typical of the previously described condition. Microscopically, the cortex layers are normal. It was first described in association with tubulinopathies and dystroglycanopathies, but the complete spectrum of disorders in which it occurs has not yet been determined (9,12,73). It is important to keep in mind that FCD type 1, FCD type 3, and secondary microcephalies are also part of group 3 (Table 1) and were previously described.

Advanced Imaging Techniques

As shown above, some MCD are subtle and may not be seen on imaging studies, possibly representing just the "tip of the iceberg." In addition to the information determined with high-spatial-resolution imaging of the cortex, diffusion tensor imaging of white matter may reveal the existence of notable changes in cerebral white matter networks (74),

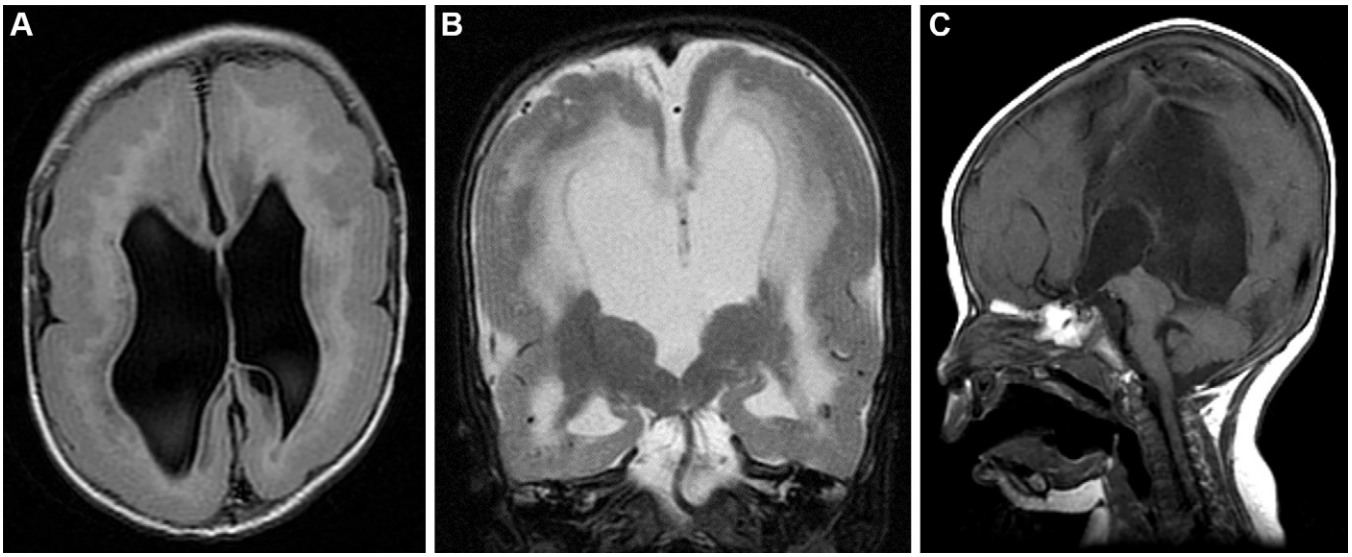

Figure 20. Walker-Warburg syndrome in an infant. **(A, B)** Axial T1-weighted **(A)** and coronal T2-weighted **(B)** MR images show the cobblestone LIS cortical pattern. **(C)** Sagittal T1-weighted MR image demonstrates a hypoplastic brainstem with a dorsal "kink" at the mesencephalic-pontine junction with a Z-shaped pattern.

Figure 21. Axial volumetric T1-weighted MR image demonstrates bilateral closed-lip schizencephaly, characterized by small clefts surrounded by PMG (arrowheads).

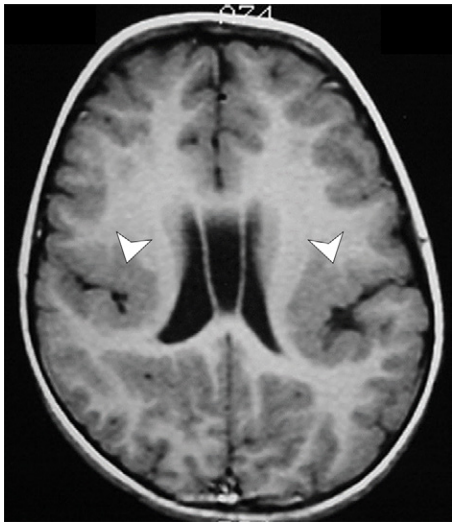

Figure 23. Dysgyria in a 4-year-old girl with developmental delay. Axial T2-weighted MR image shows an abnormal gyral pattern along the bilateral parasagittal frontoparietal lobes (arrows), with normal cortical thickness.

Figure 22. Congenital toxoplasmosis in a newborn. Axial CT image shows left open-lip schizencephaly with a big cleft connecting the subarachnoid space and ventricles. Note also the calcifications in the ventricular walls.

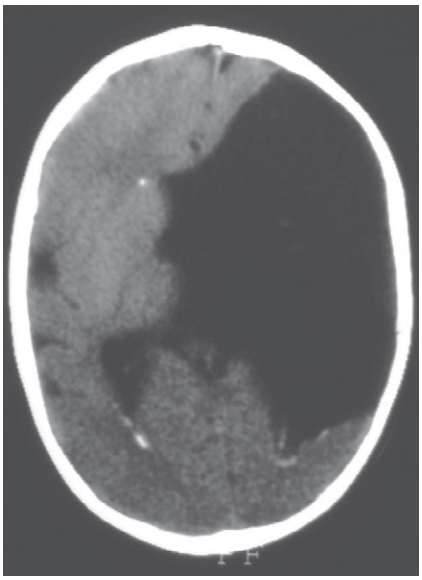

MR spectroscopy may show abnormalities in MCD lesions as well as the normal-appearing contralateral side (75), and functional MRI can delineate brain function to be used for presurgical mapping.

Conclusion

MCD are a major cause of development delay and epilepsy. The stage of embryogenesis where the disruption happens dictates how severe the condition will be. Recognizing imaging patterns is crucial in the assessment of these patients, sometimes in determining the diagnosis or at least in enabling more targeted genetic and molecular testing. Didactically, the authors provide a flowchart for a proposed imaging

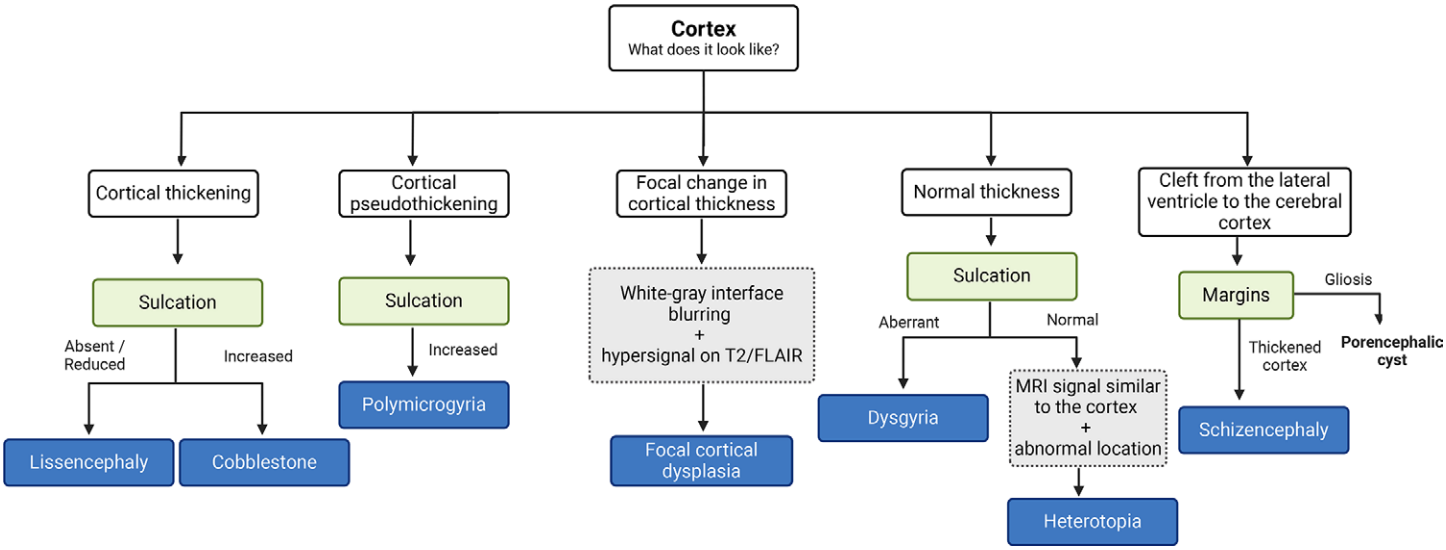

Figure 24. Flowchart summarizes the imaging approach to cortical malformations, starting from the cortical aspect of the image. (Created with BioRender.com.)

approach to MCD, which is shown in Figure 24.

Author affiliations.—From the Department of Radiology, Hospital Sírio-Libanês, Adma Jafet 91, Bela Vista, São Paulo, Brazil 01308-050 (J.M.B., T.J.P.L., I.S.A., D.S.D., H.W.L., M.G.M.M., M.F.L.D., S.S.A., P.C.P., V.T.G., J.T.T., C.T.A.); Departments of Radiology (M.G.M.M., P.C.P., L.R.L.B.O., C.C.L.) and Oncology (C.C.L.), University of São Paulo, São Paulo, Brazil; and Department of Medical Imaging, University of Toronto, Sunnybrook Health Sciences Centre, Toronto, Ontario, Canada (P.J.M.). Presented as an education exhibit at the 2022 RSNA Annual Meeting. Received December 14, 2023; revision requested January 30 and received February 27; accepted April 17. **Address correspondence to** J.M.B. (email: *juliamartinsbrunelli@gmail.com*).

Disclosures of conflicts of interest.—The authors, editor, and reviewers have disclosed no relevant relationships.

References

1. Barkovich AJ, Guerrini R, Kuzniecky RI, Jackson GD, Dobyns WB. A developmental and genetic classification for malformations of cortical development: update 2012. Brain 2012;135(Pt 5):1348–1369.
2. Moffat JJ, Ka M, Jung EM, Kim WY. Genes and brain malformations associated with abnormal neuron positioning. Mol Brain 2015;8(1):72.
3. Guérout N, Li X, Barnabé-Heider F. Cell fate control in the developing central nervous system. Exp Cell Res 2014;321(1):77–83.
4. Wong FK, Marín O. Developmental Cell Death in the Cerebral Cortex. Annu Rev Cell Dev Biol 2019;35:523–542.
5. Rakic P. Evolution of the neocortex: a perspective from developmental biology. Nat Rev Neurosci 2009;10(10):724–735.
6. Marín O, Valiente M, Ge X, Tsai LH. Guiding neuronal cell migrations. Cold Spring Harb Perspect Biol 2010;2(2):a001834.
7. Subramanian L, Calcagnotto ME, Paredes MF. Cortical Malformations: Lessons in Human Brain Development. Front Cell Neurosci 2020;13:576.
8. Zhernovaia M, Dadar M, Mahmoud S, Zeighami Y. Maranzano. PhyloBrain atlas: a cortical brain MRI atlas following a phylogenetic approach. Neuroscience 2020. https://www.biorxiv.org/content/10.1101/2020.07.15.205401. Published July 16, 2020. Accessed March 28, 2023.
9. Severino M, Geraldo AF, Utz N, et al. Definitions and classification of malformations of cortical development: practical guidelines. Brain 2020;143(10):2874–2894.
10. Dubois J, Alison M, Counsell SJ, Hertz-Pannier L, Hüppi PS, Benders MJNL. MRI of the Neonatal Brain: A Review of Methodological Challenges and Neuroscientific Advances. J Magn Reson Imaging 2021;53(5):1318–1343.
11. Barkovich AJ, Kuzniecky RI, Dobyns WB, Jackson GD, Becker LE, Evrard P. A classification scheme for malformations of cortical development. Neuropediatrics 1996;27(2):59–63.
12. Oegema R, Barakat TS, Wilke M, et al. International consensus recommendations on the diagnostic work-up for malformations of cortical development. Nat Rev Neurol 2020;16(11):618–635.
13. Ashwal S, Michelson D, Plawner L, Dobyns WB; Quality Standards Subcommittee of the American Academy of Neurology and the Practice Committee of the Child Neurology Society. Practice parameter: Evaluation of the child with microcephaly (an evidence-based review): report of the Quality Standards Subcommittee of the American Academy of Neurology and the Practice Committee of the Child Neurology Society. Neurology 2009;73(11):887–897.
14. Becerra-Solano LE, Mateos-Sánchez L, López-Muñoz E. Microcephaly, an etiopathogenic vision. Pediatr Neonatol 2021;62(4):354–360.
15. Watemberg N, Silver S, Harel S, Lerman-Sagie T. Significance of microcephaly among children with developmental disabilities. J Child Neurol 2002;17(2):117–122.
16. Adachi Y, Poduri A, Kawaguch A, et al. Congenital microcephaly with a simplified gyral pattern: associated findings and their significance. AJNR Am J Neuroradiol 2011;32(6):1123–1129.
17. Barkovich AJ, Raybaud C. Pediatric neuroimaging. 6th ed. Philadelphia Baltimore New York London Buenos Aires Hong Kong Sydney Tokyo: Wolters Kluwer, 2019: 1259.
18. de Wit MCY, de Coo IFM, Halley DJJ, Lequin MH, Mancini GMS. Movement disorder and neuronal migration disorder due to ARFGEF2 mutation. Neurogenetics 2009;10(4):333–336.
19. Takanashi J, Arai H, Nabatame S, et al. Neuroradiologic features of CASK mutations. AJNR Am J Neuroradiol 2010;31(9):1619–1622.
20. Soares de Oliveira-Szejnfeld P, Levine D, Melo ASDO, et al. Congenital Brain Abnormalities and Zika Virus: What the Radiologist Can Expect to See Prenatally and Postnatally. Radiology 2016;281(1):203–218.
21. Guerrini R, Dobyns WB. Malformations of cortical development: clinical features and genetic causes. Lancet Neurol 2014;13(7):710–726.
22. D'Gama AM, Woodworth MB, Hossain AA, et al. Somatic Mutations Activating the mTOR Pathway in Dorsal Telencephalic Progenitors Cause a Continuum of Cortical Dysplasias. Cell Rep 2017;21(13):3754–3766.
23. DeMyer W. Megalencephaly: types, clinical syndromes, and management. Pediatr Neurol 1986;2(6):321–328.
24. Mirzaa GM, Poduri A. Megalencephaly and hemimegalencephaly: breakthroughs in molecular etiology. Am J Med Genet C Semin Med Genet 2014;166C(2):156–172.
25. Flores-Sarnat L. Hemimegalencephaly: part 1. Genetic, clinical, and imaging aspects. J Child Neurol 2002;17(5):373–384; discussion 384.
26. Mirzaa GM, Conway RL, Gripp KW, et al. Megalencephaly-capillary malformation (MCAP) and megalencephaly-polydactyly-polymicrogyria-hydrocephalus (MPPH) syndromes: two closely related disorders of brain overgrowth and abnormal brain and body morphogenesis. Am J Med Genet A 2012;158A(2):269–291.
27. Mirzaa GM, Rivière JB, Dobyns WB. Megalencephaly syndromes and activating mutations in the PI3K-AKT pathway: MPPH and MCAP. Am J Med Genet C Semin Med Genet 2013;163C(2):122–130.
28. Pirozzi F, Nelson B, Mirzaa G. From microcephaly to megalenceph-

aly: determinants of brain size. Dialogues Clin Neurosci 2018;20(4): 267–282.
29. Rivière JB, Mirzaa GM, O'Roak BJ, et al; Finding of Rare Disease Genes (FORGE) Canada Consortium. De novo germline and postzygotic mutations in AKT3, PIK3R2 and PIK3CA cause a spectrum of related megalencephaly syndromes. Nat Genet 2012;44(8):934–940.
30. Kim SH, Choi J. Pathological Classification of Focal Cortical Dysplasia (FCD) : Personal Comments for Well Understanding FCD Classification. J Korean Neurosurg Soc 2019;62(3):288–295.
31. Blumcke I, Spreafico R, Haaker G, et al; EEBB Consortium. Histopathological Findings in Brain Tissue Obtained during Epilepsy Surgery. N Engl J Med 2017;377(17):1648–1656.
32. Blümcke I, Mühlebner A. Neuropathological work-up of focal cortical dysplasias using the new ILAE consensus classification system - practical guideline article invited by the Euro-CNS Research Committee. Clin Neuropathol 2011;30(4):164–177.
33. Najm I, Lal D, Alonso Vanegas M, et al. The ILAE consensus classification of focal cortical dysplasia: An update proposed by an ad hoc task force of the ILAE diagnostic methods commission. Epilepsia 2022;63(8):1899–1919.
34. Crino PB. Focal Cortical Dysplasia. Semin Neurol 2015;35(3):201–208.
35. Garner GL, Streetman DR, Fricker JG, et al. Focal cortical dysplasia as a cause of epilepsy: The current evidence of associated genes and future therapeutic treatments. Interdiscip Neurosurg 2022;30:101635.
36. Marcelis S, Vanden Bossche S, Dekeyzer S. Not Your Everyday FCD: Imaging Findings of Focal Cortical Dysplasia Type 1. J Belg Soc Radiol 2022;106(1):39.
37. Baldassari S, Ribierre T, Marsan E, et al. Dissecting the genetic basis of focal cortical dysplasia: a large cohort study. Acta Neuropathol (Berl) 2019;138(6):885–900.
38. De Ciantis A, Barkovich AJ, Cosottini M, et al. Ultra-high-field MR imaging in polymicrogyria and epilepsy. AJNR Am J Neuroradiol 2015;36(2):309–316.
39. Baron Y, Barkovich AJ. MR imaging of tuberous sclerosis in neonates and young infants. AJNR Am J Neuroradiol 1999;20(5):907–916.
40. Mata-Mbemba D, Iimura Y, Hazrati LN, et al. MRI, Magnetoencephalography, and Surgical Outcome of Oligodendrocytosis versus Focal Cortical Dysplasia Type I. AJNR Am J Neuroradiol 2018;39(12):2371–2377.
41. Schurr J, Coras R, Rössler K, et al. Mild Malformation of Cortical Development with Oligodendroglial Hyperplasia in Frontal Lobe Epilepsy: A New Clinico-Pathological Entity. Brain Pathol 2017;27(1):26–35.
42. Vuori K, Kankaanranta L, Häkkinen AM, et al. Low-grade gliomas and focal cortical developmental malformations: differentiation with proton MR spectroscopy. Radiology 2004;230(3):703–708.
43. Spitzer H, Ripart M, Whitaker K, et al. Interpretable surface-based detection of focal cortical dysplasias: a Multi-centre Epilepsy Lesion Detection study. Brain 2022;145(11):3859–3871.
44. Aronica E, Mühlebner A. Neuropathology of epilepsy. Handb Clin Neurol 2017;145: 193–216.
45. Barkovich AJ, Kuzniecky RI. Gray matter heterotopia. Neurology 2000;55(11):1603–1608.
46. Lu DS, Karas PJ, Krueger DA, Weiner HL. Central nervous system manifestations of tuberous sclerosis complex. Am J Med Genet C Semin Med Genet 2018;178(3):291–298.
47. Hiromoto Y, Azuma Y, Suzuki Y, et al. Hemizygous FLNA variant in West syndrome without periventricular nodular heterotopia. Hum Genome Var 2020;7(1):43.
48. Lu YT, Hsu CY, Liu YT, et al. The clinical and imaging features of FLNA positive and negative periventricular nodular heterotopia. Biomed J 2022;45(3):542–548.
49. Oegema R, Barkovich AJ, Mancini GMS, Guerrini R, Dobyns WB. Subcortical heterotopic gray matter brain malformations: Classification study of 107 individuals. Neurology 2019;93(14):e1360–e1373.
50. Vriend I, Oegema R. Genetic causes underlying grey matter heterotopia. Eur J Paediatr Neurol 2021;35:82–92.
51. Di Donato N, Chiari S, Mirzaa GM, et al. Lissencephaly: Expanded imaging and clinical classification. Am J Med Genet A 2017;173(6):1473–1488.
52. Koenig M, Dobyns WB, Di Donato N. Lissencephaly: Update on diagnostics and clinical management. Eur J Paediatr Neurol 2021;35:147–152.
53. Di Donato N, Timms AE, Aldinger KA, et al; University of Washington Center for Mendelian Genomics. Analysis of 17 genes detects mutations in 81% of 811 patients with lissencephaly. Genet Med 2018;20(11):1354–1364.
54. Fry AE, Cushion TD, Pilz DT. The genetics of lissencephaly. Am J Med Genet C Semin Med Genet 2014;166C(2):198–210.
55. Sandilya S, Sarkar A, Idrisi T. Lissencephaly with CMV Infection: A Case Study. Int J Clin Pharmacokinet Med Sci. 18 de dezembro de 2021;1(4):132–5.
56. Squier W, Jansen A. Polymicrogyria: pathology, fetal origins and mechanisms. Acta Neuropathol Commun 2014;2(1):80.
57. Forman MS, Squier W, Dobyns WB, Golden JA. Genotypically Defined Lissencephalies Show Distinct Pathologies. J Neuropathol Exp Neurol 2005;64(10):847–857.
58. Barkovich AJ, Dobyns WB, Guerrini R. Malformations of cortical development and epilepsy. Cold Spring Harb Perspect Med 2015;5(5):a022392.
59. Raybaud C, Widjaja E. Development and Dysgenesis of the Cerebral Cortex: Malformations of Cortical Development. Neuroimaging Clin N Am 2011;21(3):483–543.
60. Barkovich AJ. Current concepts of polymicrogyria. Neuroradiology 2010;52(6):479–487.
61. Leventer RJ, Jansen A, Pilz DT, et al. Clinical and imaging heterogeneity of polymicrogyria: a study of 328 patients. Brain 2010;133(Pt 5):1415–1427.
62. Guimaraes CVA, Dahmoush HM. Imaging phenotype correlation with molecular and molecular pathway defects in malformations of cortical development. Pediatr Radiol 2020;50(13):1974–1987.
63. Devisme L, Bouchet C, Gonzalès M, et al. Cobblestone lissencephaly: neuropatho subtypes and correlations with genes of dystroglycanopathies. Brain 2012;135(Pt 2):469–482.
64. Dobyns WB, Patton MA, Stratton RF, Mastrobattista JM, Blanton SH, Northrup H. Cobblestone lissencephaly with normal eyes and muscle. Neuropediatrics 1996;27(2):70–75.
65. Alharbi S, Alhashem A, Alkuraya F, Kashlan F, Tlili-Graiess K. Neuroimaging manifestations and genetic heterogeneity of Walker-Warburg syndrome in Saudi patients. Brain Dev 2021;43(3):380–388.
66. Hirasawa-Inoue A, Sato N, Shigemoto Y, et al. New MRI Findings in Fukuyama Congenital Muscular Dystrophy: Brain Stem and Venous System Anomalies. AJNR Am J Neuroradiol 2020;41(6):1094–1098.
67. Shenoy AM, Markowitz JA, Bonnemann CG, Krishnamoorthy K, Bossler AD, Tseng BS. Muscle-Eye-Brain disease. J Clin Neuromuscul Dis 2010;11(3):124–126.
68. Brun BN, Mockler SRH, Laubscher KM, et al. Comparison of brain MRI findings with language and motor function in the dystroglycanopathies. Neurology 2017;88(7):623–629.
69. Jerber J, Zaki MS, Al-Aama JY, et al. Biallelic Mutations in TMTC3, Encoding a Transmembrane and TPR-Containing Protein, Lead to Cobblestone Lissencephaly. Am J Hum Genet 2016;99(5):1181–1189.
70. Vandervore L, Stouffs K, Tanyalçin I, et al. Bi-allelic variants in COL3A1 encoding the ligand to GPR56 are associated with cobblestone-like cortical malformation, white matter changes and cerebellar cysts. J Med Genet 2017;54(6):432–440.
71. Stopa J, Kucharska-Miąsik I, Dziurzyńska-Białek E, et al. Diagnostic imaging and problems of schizencephaly. Pol Przegl Radiol Med Nukl 2014;79:444–449.
72. Gutierrez-Castillo A, Jimenez-Ruiz A, Chavez-Castillo M, Ruiz-Sandoval JL. Septo-optic Dysplasia Plus Syndrome. Cureus 2018;10(12):e3727.
73. Mutch CA, Poduri A, Sahin M, Barry B, Walsh CA, Barkovich AJ. Disorders of Microtubule Function in Neurons: Imaging Correlates. AJNR Am J Neuroradiol 2016;37(3):528–535.
74. Li CCT, Yin H, Loh NK, Chua VGE, Hui F, Barkovich AJ. Malformations of cortical development: high-resolution MR and diffusion tensor imaging of fiber tracts at 3T. AJNR Am J Neuroradiol 2005;26(1):61–64.
75. Leite CC, Lucato LT, Sato JR, Valente KD, Otaduy MCG. Multivoxel proton MR spectroscopy in malformations of cortical development. AJNR Am J Neuroradiol 2007;28(6):1071–1075; discussion 1076–1077.